GIS-based topographic reconstruction and geomechanical modelling of the Köfels Rock Slide

Christian Zangerl[1], Annemarie Schneeberger[1,2], Georg Steiner[1,3], Martin Mergili[1,4]

[1]Institute of Applied Geology, University of Natural Resources and Life Sciences (BOKU), Vienna, 1190 Austria
[2]Institute of Geography, University of Innsbruck, Innsbruck, 6020, Austria
[3]Amt der Kärntner Landesregierung, Klagenfurt, 9021, Austria
[4]Department of Geography and Regional Science, University of Graz, Graz, 8010, Austria

Correspondence to: Christian Zangerl (christian.j.zangerl@boku.ac.at)

Abstract.

The Köfels Rock Slide in the Ötztal Valley (Tyrol, Austria) represents the largest known extremely rapid landslide in metamorphic rock masses in the Alps. Although many hypotheses for the trigger were discussed in the past, until now no scientifically proven trigger factor has been identified. This study provides new data about the i) pre-failure and failure topography, ii) failure volume and porosity of the sliding mass, and ~~and~~ iii) numerical models on initial deformation and failure mechanism, as well as shear strength properties of the ~~gneissic rock mass~~basal shear zone obtained by back-calculations. Geographic information system methods were used to reconstruct the slope topographies before, during and after the event. Comparing the resulting digital terrain models leads to volume estimates of the failure and deposition masses of 3.1 km³ and 4.0 km³, respectively and a sliding mass porosity of 26%. For the 2D numerical investigation ~~For the back-calculations the 2D discrete~~ the distinct element method was applied to study the geomechanical characteristics of the initial failure process (i.e. model runs without a basal shear zone) and to determine the shear strength properties of the reconstructed basal shear zone. Based on numerous model runs by varying the block and joint input parameters the failure process of the rock slope could be plausibly reconstructed, however, the exact geometry of the rock slide, especially in view of thickness, could not be fully reproduced. Our results suggest that both failure of rock blocks and shearing along moderately to east dipping joints were responsible for the formation or the rock slide. The progressive failure process may have taken place by fracturing and loosening of the rock mass, advancing from shallow to deep-seated zones, especially by the development of internal shear zones as well as localised domains of increased block failure. The simulations further highlighted the importance of considering the dominant structural features of the rock mass. Considering back-calculations of the strength properties i.e. the friction angle of the basal shear zone, results ~~Results~~ indicated that under no groundwater flow conditions, an exceptionally ~~very~~ low friction angle ~~below24°~~of 21° to 24° or below is required to promote failure, depending on how much internal shearing of the sliding mass is allowed. Model runs considering ~~, whilst, with~~ groundwater flow resulted in approx. 6° higher back-calculated critical friction angles ranging from 27° to 30°. ~~, the critical value increase to 28°.~~ Such ~~a~~ low friction angles of the basal failure zone are~~is~~ unexpected from a rock mechanical perspective for this strong rock and groundwater flow, even if high water pressures are assumed, may not be able to trigger this rock slide. In

addition, the rock mass properties needed to induce failure in the model runs if no basal shear zone was implemented are significantly lower than those which would be obtained by classical rock mechanical considerations. Additional conditioning and triggering factors ~~should be identified by further studies, for example focussing on~~such as the impact of earthquakes acting as precursors for progressive rock mass weakening may have been involved to cause this gigantic rock slide. ~~the impact of dynamic loading~~.

1 Introduction

In mountain areas, life and property are often put at risk by landslide processes (e.g., Dai et al. 2002; Nadim et al. 2006; Margottini et al. 2013; Sassa et al. 2014). Rapid collapses of huge mountain slopes – and resulting process chains – have repeatedly evolved into catastrophic events (e.g., Evans and DeGraff 2002; Govi et al. 2002; Genevois and Ghirotti 2005; Evans et al. 2009a,b). An adequate understanding of the mechanisms of the initial failure and extremely rapid movement processes is one key for the implementation of effective risk reduction strategies. The analysis of past – even fossil – events may contribute to a better understanding of landslide processes and therefore help to develop and to improve methods for hazard and risk mitigation (Kilburn and Pasuto 2003).

Known as the largest landslide in metamorphic rock throughout the European Alps, the Köfels Rock Slide represents such a fossil landslide (see Section 2 for a detailed description). In contrast to numerous deep-seated rock slides in foliated metamorphic rocks characterised by movement rates of a few centimetres to decimetres per year and without indications of total slope failure (Zangerl et al. 2015), the Köfels Rock Slide is a prominent case study for a sudden slope failure with extremely rapid movement velocities. This can be clearly demonstrated by the occurrence of frictionites which were found at outcrops on the deposited sliding mass (Erismann et al. 1977). Even though this giant landslide has been subject of numerous studies focussing on the genesis of the frictionites, age of the event, spatial distribution of the source area, volume of the rock slide mass, and geomechanical aspects concerning the trigger and failure mechanisms (e.g., Pichler 1863; Milton 1964; Preuss 1974, 1986; Erismann et al. 1977; Preuss et al. 1987; Erismann and Abele 2001; Brückl et al. 2001, 2010; Brückl and Parotidis 2001, 2005; von Poschinger 2002; Sørensen and Bauer 2003; Prager et al. 2009, Nicolussi et al. 2015), the conditioning and triggering factors of the Köfels Rock Slide remain still unknown and speculative.

Computer models focussing on the rock slide geometry and geomechanical processes may help to increase our understanding of the mechanisms of rock slope failure. Although models are always a rough simplification of reality, some are useful (Box and Draper 1987) to explore specific aspects such as rock slide volumes, slope deformations or critical values of geomechanical parameters at failure. In the context of this study two types of models, i.e. topographical and geomechanical models, are relevant. Brückl et al. (2001) were the first ones who reconstructed the 3D pre-failure topography and failure geometry of the Köfels Rock Slide on the basis of seismic measurements and terrain models and they derived parameters such as failure and deposition volumes, porosity, the initial and average sliding angles and the release of potential energy.

In our study we used new high-resolution (1 m raster data) airborne laser scanning (ALS) based digital terrain models, new geological mapping data and pre-existing data from seismic measurements to re-build and re-analyse the pre- and post-failure topographies and geometries of the rock slide. Based on this topographic reconstruction by using geographic information system (GIS) analysis methods a geometrical-kinematical rock slide model were developed. Conclusions can be made about the failed and deposited volumes, and consequently, the change of rock mass porosity induced by the rapid sliding and fracturing and loosening processes.

Concerning geomechanics of the rock slide at initial failure state and movement several attempts were made to investigate the mechanisms and to back-calculate rock mass properties. Erismann et al. (1977) developed a kinematic and thermodynamic model to explain the energy release necessary for the formation of the frictionites that were found at the Köfels site (see Section 2). Brückl and Parotidis (2001) set up a 2D elastic and elasto-plastic continuum model to estimate the geomechanical rock mass properties of the Köfels Rock Slide. In their approach they applied the 2D finite element method to explore the initial phase of the failure process by studying creeping and strength degradation of the rock mass. The model suggests that the Köfels Rock Slide was formed due to progressive strength softening of the rock mass, which initiates at the foot of the slope and propagates uphill. Furthermore, the model calculations determined surprisingly low friction angles of the rock mass, ranging between 20–24° to induce slope failure. In another approach, Brückl and Parotidis (2005) proposed a model with focus on time-dependent strength degradation and slope failure under low stress regimes such as rock mass creep and subcritical crack growth. They suggest that subcritical crack growth is a primary geomechanical process which, after glacier retreat, is able to explain the considerable rock mass strength weakening needed for failure.

However, the extraordinary low strength properties of the rock mass that were back-calculated by 2D continuum approaches for the failure state raise questions:

- Can we plausibly reconstruct the topography to provide a realistic pre-failure topography for the geomechanical modelling?
- How could the initial failure process have taken place?
- How can the strength of such a strong granitic rock mass reduce to such small values needed to promote failure?
- ~~Why do we observe only one such giant and extremely rapid rock slide characterised by a flat to moderately dipping failure surface in Ötztal-Stubai crystalline basement?~~
- Are there any structural particularities in the Köfels Rock Slide area that may have contributed to slope failure and how is the influence of the pre-existing fracture network?~~?~~
- Why do we observe only one such giant and extremely rapid rock slide characterised by a flat to moderately dipping failure surface in Ötztal-Stubai crystalline basement?

Given that, so far, only 2D continuum models have been applied to ~~reconstruct~~ investigate the failure mechanisms of the Köfels Rock Slide we believe that, though representing a valid approach, additional types of models, e.g. discontinuum models, are useful to adequately capture the complexity of the phenomenon. Discontinuum models such as the distinct element method have the advantage that the geometry of the rock slide mass and the discrete basal shear zone can be implemented directly

Formatiert: Nicht Hervorheben

based on geometrical and structural field observations and GIS-reconstructions. Geomechanically, the basal shear zone i.e. stepped rupture surface can be considered in the model as a discrete narrow zone. In order to fill this gap, we set up a 2D discontinuum model of the Köfels Rock Slide, based on the geometry obtained by the topographic ~~model~~reconstruction, and by applying the ~~discrete~~ Universal Distinct Eelement Ccode UDEC by Itasca (Itasca Consulting Group ~~2014b~~2020). The initial failure process was studied by considering the main structural characteristics based on geological field surveys. The aim was to investigate how the rock slide geometry and the basal shear surface (zone) was formed during the initial failure process. In addition, ~~Back~~back-calculations of the critical angle of friction along the basal shear zone assuming no groundwater flow conditions and groundwater flow are conducted under quasi-static conditions. These back-calculations were done to determine the shear strength properties, i.e. friction angle and cohesion, of the predefined and field-based basal shear zone needed to promote failure. The models were performed to explore the influence of fracture water pressure in the rock mass and basal shear zone resulting from ~~exceptional~~ high groundwater levels for provoking this giant landslide.

~~In addition to the back-calculation of shear strength properties at failure,~~The numerical modelling study was supplemented by a geological field survey ~~was performed to~~ searching for instability-relevant discontinuities of different origin and scale. This was done to investigate the impact of discontinuities which ideally are dipping moderately towards east, acting as weakness zones and thus reducing the overall rock mass strength. Particular focus was given on the identification of low-strength brittle fault zones composed of gouges and breccia characterised by a high persistence.

Next, we introduce to the study area, the Köfels Rock Slide (Section 2). Then, we explain the methods applied for the topographic reconstruction and geomechanical modelling (Section 3). We present (Section 4) and discuss (Section 5) the results before concluding with the key messages of this study (Section 6).

Formatiert: Nicht Hervorheben

Formatiert: Nicht Hervorheben

Formatiert: Nicht Hervorheben

Formatiert: Nicht Hervorheben

Formatiert: Nicht Hervorheben

Formatiert: Nicht Hervorheben

Formatiert: Nicht Hervorheben

Formatiert: Nicht Hervorheben

2 Study area and data

2.1 Geographic and geologic setting

The Köfels Rock Slide (Figs. 1 and 2) occurred in the central part of the north-south striking Ötztal Valley (Tyrol, Austria), at present at an elevation between 950 m and 1100 m asl. Surrounded by up to 3.000 m high summits, this area is deeply incised in the polymetamorphic Ötztal complex, a major thrust unit belonging to the Upper Austroalpine basement nappes (Prager et al. 2009). Lithologically, different types of metamorphic rocks i.e. paragneisses, quarzites and micaschists with intercalations of orthogneisses, amphibolites and eclogites are encountered (Hammer, 1929; Purtscheller, 1978). The complex ductile and brittle structural setting results from polyphase and heteroaxially deformations and is attributed to at least three distinct orogeneses and their corresponding regional metamorphic overprint. In contrast to numerous petrological and geochronological studies, the brittle deformation history and their related structures of the Ötztal basement was not studied so far in detail, but would be highly relevant for geomechanical purposes. However, Prager et al. (2009) provide some data concerning the discontinuity network in the surroundings of the Köfels Rock Slide.

During the Quaternary period, the Ötztal valley was influenced by repeated glacier fluctuations, causing valley incision, glacial and fluvial erosion as well as sediment accumulation. Valley deepening and steepening leads to substantial stress redistributions in the rock slopes, which in turn initiates time-dependent progressive failure processes in the fractured rock mass and may expose preferentially orientated failure surfaces.

2.2 The Köfels Rock Slide

The age of the Köfels Rock Slide was determined several times through radiocarbon dating of wood buried by the rock slide deposits (Ivy-Ochs et al. 1998), surface exposure dating of rock slide boulders (Kubik et al. 1998) and actually by tree-ring analysis and radiocarbon dating of new wood samples (Nicolussi et al. 2015). The last dating campaign, yielding 9527–9498 cal BP, led to a significant refining of the timing of the Köfels landslide event and even was able to constrain the season during which the event occurred.

The main source of the slide is located in competent fractured orthogneisses (Augengneiss) around the small village Köfels. Only at the southern head scarp area the failure mass is composed of paragneissic rock. The head scarp located at the western slope of the central Ötztal Valley is very steep with inclinations of up to 40–80°. Comprising a failure volume of more than 3 km^3 the Köfels Rock Slide poses a particular event of very rapid large-scale failure in metamorphic rock mass (Brückl et al. 2001). Typically, such rapid rock slides characterised by a moderately inclined basal failure surface occur in carbonatic rock masses (Prager et al. 2008). The displacement of the sliding rock mass initiated at the east facing slope south of Wenderkogel (see Fig.1 and 2) and stopped at the opposite slope in the east at the entrance of the tributary valley Horlachtal Valley, where it collided with massive bedrock. The centre of mass displacend around 2.6 km (Sørensen and Bauer 2003), reaching a velocity of approx. 50 m/s (Erismann et al. 1977). The main rock slide deposit blocked the Ötztal Valley and formed a prominent valley spur of fractured and disintegrated orthogneiss. Erismann and Abele (2001) proposed that the mass was split into two parts with the lower one arresting due to the collision within the steep valley slope and the upper one which continued its movement, thus creating an additional internal sub-horizontal shear zone. The Taufer~~b~~erg (see Figs.1 and 2) was formed when the upper mass continued its movement towards the Horlachtal valley for approx. one more kilometre and ran up for approx. 100 m. Though plausible, evidence for a distinct internal shear zone was claimed by Preuss (1986), but proof for the existence of such a feature has not yet been found in the field. It seems even more plausible that the immense internal rock mass deformation during the movement and the adaptation to the terrain surface was based on the formation of numerous internal shear zones. The disintegration of the rock mass during the slide event caused a very heterogeneous highly fractured and partly crushed rock mass, with shear zones composed of gouges and breccias and zones with blocks of more than 10 m diameter (Sørensen and Bauer 2003). Furthermore, zones that are characterised by high fracture frequencies only marginally increased in comparison to those commonly observed in undisturbed fractured rock masses. This distinctive fragmentation of rock led to radon gas emissions and locally radioactive springs, which still affects today's population in Umhausen and causes noticably high cancer rates (Purtscheller et al. 1995).

After the slide event, a temporary lake flooded the basin of Längenfeld, impounded by the valley spur (Ampferer 1939). As a result of the flooding backwater sediments were deposited in the basin of Längenfeld as well as in the blocked tributary Horlachtal Valley at Niederthai. According to drilling data from von Klebelsberg (1951) and Ampferer (1939), the lacustrine sediments reach a maximum thickness of 92 m. Later on, the river Ötztaler Ache cut into the rock slide deposits, forming the Maurach gorge by fluvial erosion (see Figs. 1 and 2; Erismann and Abele 2001).

When the mountain slope collapsed, an amount of about $1.6x10^{16}$ J of energy was released. This value was estimated by Erismann and Abele (2001) with respect to volume, density and vertical displacement of the rock mass. The high amount of released energy led to partial melting of the orthogneissic rock at the progressively exposed sliding surface but also around internal shear zones and the development of a fused rock (i.e. pumice, frictinites, hyalomylonites), the presence of which was interpreted in various ways over the years (e.g., Pichler 1863; Preuss 1974; Erismann et al., 1977; Masch et al., 1985; Weidinger et al. 2014).

Though subject of research for more than one century, the question of the causes and maybe the "single" trigger for the Köfels Rock Slide remains still open. Most probably a combination of various conditioning and interacting triggering factors led to the release of this giant slide.

Given that the collapse of Köfels occurred >5 ka years after valley deglaciation, time-dependent progressive failure processes such as sub-critical crack growth and fracture propagation were caused by over-steepening of the valley flanks which is assumed to have provoked unstable conditions in the slope. This long-term disintegration of rock is seen as a prerequisite for the development of a large-scale rock slide (Prager et al. 2009, Brückl and Parotidis 2005, Abele 1994). Moreover, permafrost degradation is suspected to have influenced the failure of many Holocene deep-seated rock slides (Abele 1994) - a phenomenon that gains new relevance considering the degrading permafrost in today's mountains influenced by modern climatic changes (e.g. Gruber and Haeberli 2007, Huggel et al., 2010)~~. To what extent permafrost degradation is able to trigger a deep-seated rock slides characterised by a shear zone at a depth of several hundred metres, is unclear and still under discussion (Nicolussi et al. 2015)~~. Abele (1994) and Weidinger (2006) describe active tectonics i.e. earthquakes as one main background condition provoking large rock slide events due to dynamic loading. Considering the present low seismic activity in the Ötztal Valley, Sørensen and Bauer (2003) question an earthquake as a possible trigger for the event.

2.3 Data

An up-to-date digital elevation model (DEM), gained by airborne laser scanning (LiDAR), of the investigated area was obtained from the governmental service for maps of Tyrol, TIRIS, at a spatial resolution of 1 m. Topographic and geologic information on the situation before and after the Köfels Rock Slide are given through studies of von Klebelsberg (1951), Brückl (2001), Heuberger (1994) and Prager et al. (2009). Data from several boreholes from von Klebelsberg (1951) were used in this work. Additionally, reflection and refraction seismic measurements were conducted between 1986 and 1990 (Brückl 1988; Brückl and Heuberger 1993; Brückl et al. 1998; Brückl et al. 2001). In the framework of a hydroelectric power project an investigation drift was drilled into the Taufer~~B~~erg in 1952 and provides additional information about the geological setting

of the site (Brückl et al. 2001; Ascher 1952). Figure 3 provides an overview of the geophysical and drilling data used for the study.

3 Methods

3.1 Reconstruction of rock slide topography, volume and porosity

Three topographic profiles were constructed, based on the drilling and seismic data provided by von Klebelsberg (1951), Heuberger (1994) and Brückl et al. (2001): Profile 1 is set north of the rock slide zone through the basin of Umhausen, Profile 2 lies within the sliding surface, and profile 3 south of the rock slide zone in the basin of Längenfeld (see Figs. 2 and 3).

Fig. 2 and 3 shows the SWW-NEE Profiles 1 and 3. The two profiles display the pre-failure topography reconstructed from the seismic and borehole data and the up-to-date situation. The seismic profiles were projected to the topographic sections and transformed into point data used as input for the GIS-based topographic reconstruction. All spatial analysis tasks were performed using the ArcGIS software by ESRI.

For the reconstruction of the past topographic scenarios, an intermediate horizon of the reflection seismic data was assumed as the top of compacted sediments made up of an old valley infill, which was interpreted to be older than the Köfels Rock Slide. These sediments were buried by the rock slide mass and their upper boundary used for the reconstruction of the topographic scenario in the valley as it was before the Köfels Rock Slide. The deepest horizon with a maximum depth of 400 m was interpreted as the compact rock surface – identical with the sliding plane of the rock slide at the flanks of the valley (Brückl et al. 2001).

The available data are then used to three-dimensionally reconstruct four topographic situations, assuming a U-shaped pre-failure valley topography as well as a curved failure surface:

1. the pre-failure topography before the Köfels Rock Slide event and before the alluvium north and south of the site was deposited;
2. the topography of the failure surface with the deposits completely removed from the model to illustrate the basal shear zone and without the alluvial deposits north and south of the rock slide;
3. the post-failure topography without the alluvial deposits and with the Köfels Rock Slide deposit in the valley before the incision by the Ötztaler Ache;
4. the up-to-date topography where the Maurach gorge has been created by the incision of the Ötztaler Ache into the deposits and the alluvium has been deposited in the basins of Längenfeld and Umhausen (see Fig. 2).

Within the rock slide mass only information from seismic lines and the investigation adit was given. In the failure area only few data were available. The reconstruction of the pre-failure topography of the Köfels Rock Slide was built on the contour lines of the escarpment of the up-to-date DEM. The hypothetic pre-failure slope between the edges of the escarpment was assumed plane. This simple way of reconstruction does not require additional assumptions not supported by observations.

The failure and the deposition volumes of the Köfels Rock Slide mass were computed from the three reconstructed DEMs:

$$V_F = \sum_{i=1}^{i=m} A(zi,_1 - z_{i,2}), \quad (1)$$

$$V_D = \sum_{i=1}^{i=m} A(z_{i,3} - z_{i,2}), \quad (2)$$

where V_F and V_D are the failure and deposition volumes, and $z_{i,1}$, $z_{i,2}$ and $z_{i,3}$ represent the reconstructed elevation of the pixel *i*, the numbers referring to the stages given above. *A* is the area of one pixel, *m* is the number of pixels.

Based on the results of the volumetric calculation in ArcGIS, the porosity of the rock mass before and after failure of the Köfels Rock Slide was estimated. Porosity is defined as the ratio of void space to the total volume of soil or rock (Fetter 2001):

$$n = \frac{V_p}{V_s + V_p}, \quad (3)$$

where *n* is the porosity, V_p is the volume of void space and V_s is the volume of solids.

3.2 Discontinuity mapping and rock mass characterisation

In order to characterise the discontinuity network and the rock mass strength a field survey based on outcrop- and scanline mapping was performed at the slopes of the head scarp. Particular focus was given to detect brittle fault zones composed of gouge and breccia, which are dipping moderately towards east and therefore could have acted, at least partly, as the basal shear zone of the Köfels Rock Slide. Estimation of rock mass strength and shear strength of discontinuities was done to provide data for the comparison with results obtained by the numerical modelling study.

3.3 Distinct element modelling of the Köfels Rock Slide ~~Back-calculation based on a discontinuum model (2D)~~

3.3.1 Modelling strategy

A discontinuum model (i.e. distinct or discrete -element method) has not yet been applied for geomechanical modelling of the Köfels Rock Slide (see Section 1). The major advantage of discontinuum modelling compared to a classical continuum approach, is that i) the structural anisotropy of the rock mass caused by a discrete fracture network can be considered, and ii) typically for slides, a distinct, field-based and in relationship to the model size a thin ~~and discrete~~ basal sliding zone, which is able to accumulate large shear displacements, can be implemented and modelled.

In this study we performed more than 50 model runs and established two types of distinct element model scenarios I and II. Model scenario I was built to investigate the initial failure mechanism of the rock slide, primarily characterised by internal deformation of the slope and the development of the fully-persistent basal rupture surface (shear zone). To achieve this, the model considered the main characteristics of the in-situ fracture network (i.e. shear and opening displacements) as well as rock block deformation and failure (i.e. the Mohr-Coulomb constitutive model). However, a basal shear zone was not implemented. Model scenario II was built to perform ~~performed~~ back-calculations of the shear strength properties of the basal shear zone at failure state. Both scenarios were calculated either by considering dry conditions or groundwater flow by applying a water

Formatiert: Nicht Hervorheben

pressure in the discontinuities. ~~(i.e. critical angle of friction φ_{bs} by assuming a cohesion c_{bs}=0 MPa) of the basal shear zone at failure (A) without pore water pressure and (B) with pore water pressure, induced by ground water flow. We expected the results~~The aim of this modelling campaign was,

a) to study the initial failure mechanism before the basal rupture zone was formed,
b) to assess the impact of the pre-existing fracture network on the failure geometry of the rock slide,
c) to investigate the role of discontinuity and rock block properties, and constitutive relationships,
d) to back-calculate the shear strength properties of the basal shear zone at the failure state and its bandwidth under the framework of the comprehensively reconstructed pre-failure topography,
e) to determine internal deformation behaviour of the rock slide mass and the influence of the shape of the basal shear zone on it,
f) to allow conclusions on the role of water pressure as a possible trigger mechanism of the event, by evaluating the required shear strength properties against typical values of fractured rock masses,

Formatiert: Nummerierte Liste + Ebene: 1 + Nummerierungsformatvorlage: a, b, c, … + Beginnen bei: 1 + Ausrichtung: Links + Ausgerichtet an: 0,63 cm + Einzug bei: 1,27 cm

Formatiert: Einzug: Links: 1,27 cm, Keine Aufzählungen oder Nummerierungen

~~1. to enable estimations to be made of the bandwidth of φ_{bs} for the field based failure surface under the framework of the reconstructed pre-failure topography;~~
~~2. to allow conclusions on the role of increased pore water pressure as possible trigger mechanism of the event by evaluating φ_{bs} against typical values of φ of the rock materials and structures involved;~~
~~3. to serve as a basis for future analyses such as the impact of dynamic loading on slope stability and its potential for the triggering of the Köfels Rock Slide.~~

For the numerical study a two-dimensional distinct element model based on the code UDEC (Itasca ~~2014~~2020) was designed. This software tool characterizes a discontinuous rock mass by an assembly of discrete blocks with contacts or interfaces in between. A continuum mesh of finite-difference zones ~~defines~~ provides the deformability of the ~~rock mass~~blocks according to elastic or elasto-plastic constitutive models. During the calculation procedure the deformable blocks interact mechanically at their surfaces and corners. Block velocities and displacements are determined, with the calculation procedure being repeated until a balanced state of equilibrium or ongoing failure is reached.

~~**3.3.2 Model geometry, boundary and initial conditions**~~

~~Profile 2 (see Fig. 2 and 3) was taken for the discrete element (UDEC) modelling. The pre-failure topography was implemented to create the surface of the slope, whilst the topography of the sliding surface provides the input for the basal shear zone (Fig. 5). Blocks were considered as linear elastic defined by Hooke's law, considering components of stress to be linear functions of components of strain (Jaeger et al., 2007). The main deformation within the system takes place through the movement along discontinuities, i.e. shear and normal displacement. Sliding and rotation of blocks, and opening and interlocking of interfaces make up the movement of the mass (Itasca 2014).~~

~~Spacing of the joint set was assumed 50 m in the rock slide mass and 150 m in the underlying granitic gneiss block (see Fig. 5). The finite difference mesh in the model was assigned by a size of 25 m in the rock slide mass and 50 m in the underlying granitic gneiss block. Rounding of block corners were applied with a radius of 0.5 m. This avoids the problem of contact overlap, possibly resulting from the interaction of blocks occurring close to or at two opposing block corners (Itasca 2014).~~

~~In the modelling scenario (B) a groundwater table was assumed with respect to characteristic groundwater flow patterns where the unsaturated zone between the surface and the water table is typically deep at the head of the slope, whereas the water table at the basis of the slope is close to or at the surface (see Fig. 5; e.g. Fetter 2001).~~

~~No displacement boundaries were applied on the left, right and lower model boundary (Fig. 5). For models with pore water pressure (B), the lower model boundary was set to a no flow i.e. impermeable boundary. The left and right groundwater model boundary was defined by a hydraulic gradient based on hydrostatic water pressure according to the assumed water table. The maximum water pressure was set to 19.7 MPa at the left boundary along the y-axis and to 8.98 MPa at the right boundary along the y-axis (see Fig. 5). The in situ stresses were initialised in terms of a vertical gradient based on gravity and the horizontal stresses being half of the vertical stresses by assuming a k-ratio of 0.5. At the model origin (0,0) the two horizontal stresses were assigned to σ_{xx} = σ_{zz} = 25.6 MPa and the vertical stress to σ_{yy} = 51.2 MPa, respectively.~~

~~3.3.3 Material properties~~

~~The back-calculations of the friction angle of the basal shear zone were conducted with the assumption of the discontinuities of φ = 30° (c=0 MPa) for the granitic gneiss of the failure mass and the underlying block (Table 1). The friction angle of the basal shear zone was varied between 20° and 27° for (A) and between 25° and 32° for (B), by assuming a cohesion of c=0 MPa. A density of ρ = 2,600 kg/m³ was assigned to all rock materials. Assuming a Young's modulus E = 40 GPa and a Poisson's ratio ν = 0.2 a bulk modulus of 17 GPa and the shear modulus of 22 GPa of the granitic gneiss was obtained. Simplified conditions with a vertical and horizontal fully persistent joint set were implemented to simulate isotropic groundwater flow conditions for (B). Table 1 summarizes the material properties applied to the model.~~

4 Results

4.1 Reconstruction of rock slide topography, volume and porosity

Figs. 5~~6~~ and 6~~7~~ illustrates the results of the three-stage topographic reconstruction of the Köfels Rock Slide. Whilst stage 2 represents a theoretical situation that has never occurred in this way (however, it is necessary to reconstruct the rock slide volumes, see Eqs 1 and 2), the stages 1 and 3 represent hypothetic morphologies directly before and after the event. Note that the very smooth pre-failure topography of the failure area most probably does not resemble the original shape of the mountain slope before failure (see Figs. 5~~6~~ and 6~~7~~a) – however, given the fact that there are no data supporting more advanced reconstruction methods, we considerd this approach a reasonable approximation. Stage 4 represents the situation observed today. Comparing Figs. 6~~7~~c and d indicates those morphologic processes having shaped the site since the event, most

significantly the incision of the Maurach gorge by the Ötztaler Ache River into the rock slide deposits and the deposition of lake sediments in the basins of Umhausen and Längenfeld as well as the Horlachtal Valley (see Figs. 1, 2 and ~~6~~5).

Applying the Eqs. 1 and 2 to the reconstructed topographies, a failure volume of V_F = 3.1 km^3 and a deposition volume of V_D = 4.0 km³ were obtained (Fig. 7~~8~~). Based on these volumetric reconstructions of failure and deposition masses, considerations about the porosity before and after the Köfels Rock Slide were made. Typical porosities for intact granitic rocks caused by micro-fractures are around 1–2%, not considering any meso-scale joints (Zangerl et al. 2003). Taking into account joints in the rock mass the porosity increase to 2–5% (Fetter 2001). Assuming a pre-failure porosity of the fractured granitic rock mass of 5% and a constant volume of the solid content of the rock mass V_s before and after the collapse of the mountain slope, Eq. 3 predicts a porosity of the fractured rock mass after the sliding event of approx. 26%. Consequently, we estimated an increase of the mean porosity from a few % to 26% resulting from the disintegration of the rock mass during the Köfels Rock Slide.

4.2 Discontinuity and rock mass characterisation

The overall structural setting of the Köfels rock slide scarp area has already been comprehensively described in Prager et al. (2019). Nevertheless, in this study new discontinuity data were obtained during an outcrop mapping campaign in the orthogneissic rocks around the central part of the head scarp. Data comprising discontinuity orientation, frequency, spacing, length, roughness and strength were sampled by scanline and outcrop surveys to determine the structural anisotropy and to estimate roughly the strength properties of the rock mass. The orthogneissic rock is foliated, therefore highly anisotropic with a mean dip direction and dip angle of 114/07 (Fig. 1c). At meso-scale, the rock mass is fractured by four joint sets. One primary joint set, labelled as set #1 is dipping moderately towards east varying around a mean dip direction/dip angle of 090/32 (Fig. 1c). Joints assigned to set #1 are dipping sub-parallel to the exposed scarp surface and thus are part of the basal shear zone/surface. Remarkably, these joints feature a medium to very high persistence reaching lengths of several tens of metres and a surface roughness defined as rough and stepped (ISRM 1978). According to the approach of Barton and Choubey (1977) a mean joint roughness coefficient of JRC=10 was determined. Occasionally, some surfaces of fractures orientated sub-parallel to set #1 are coated with Quartz minerals, representing vein fillings which were most likely sheared and exposed during the rock slide events. The appearance of striations on these fractures suggest a tectonic origin, i.e. shear fractures/fault planes. A further dominant joint set (#2) is dipping steeply towards WSW (dip direction/dip angle of 242/70, Fig. 1c). However, in some areas surrounding the head scarp set #2 dips steeply towards east (Fig. 1c). The stepped topography of the scarp flank observed in the upper scarp area originated by intersection of these two joint sets, forming a stepped failure surface. In addition, two less prominent joint sets i.e. set #3 clustering around a mean of 133/47 and overlapping with set #1 as well as set #4 with a mean of 030/65 were measured (Fig. 1c).

Based on field measurements in the orthogneissic rock mass a mean total joint spacing of around 0.6 m and a mean block size of approximately V_b=0.3 m^3 were obtained. Special attention was given during the field campaigns to detect brittle fault zones of tectonic origin with a preferable orientation, dipping moderately to east and with fault zone infillings of gouge and breccia.

These brittle fault zones, if available, could have acted as low-strength weakness zones and therefore been responsible to a certain degree for the rock slide formation. Although a detailed exploration of the terrain was carried out, no such structures could be found. In addition, the spatial analysis of high-resolution LiDAR-based digital elevation models (DEM, 1 m raster) provide also no evidence for such brittle faults. On the contrary, most brittle fault zones mapped are inclined steeply and are striking WNW-ESE (major set), ENE-WSW (minor) and NNW-SSE. As already mentioned above, only meso-scale fractures coated with striations were found in the scarp area, representing structures with shear markers. Based on the current level of knowledge there is no evidence that low-strength brittle fault zones were involved as part of the basal rupture surface in the initial progressive failure process of the rock slide.

In order to assess the strength of the rock mass, the GSI characterisation method proposed by Cai et al. (2004) and Hoek and Brown (1997) was applied. From field survey a GSI≥55 and from block size/joint spacing a GSI=55 were obtained for the orthogneissic rock. Uniaxial compressive tests performed on orthogneisses show a mean UCS value of 125 MPa (9 tests were performed on similar rocks in the context of a dam project). In order to consider the influence of long-term loading on the strength of the intact rock (rock creeping, sub-critical crack growth) the uniaxial compressive strength is reduced to 40% of the test results, which yields 50 MPa (Damjanac and Fairhurst, 2010). In order to assess the lower limit of the rock mass strength, the GSI was further reduced to 45 by assuming an intact rock parameter m_i=15 (Hoek and Brown, 1997). Based on these parameters and the Hoek-Brown failure criterion a rock mass shear strength of c_{rm}=2 MPa and φ_{rm}=35° was obtained. The intact rock shear strength of orthogneissic rock was determined by triaxial laboratory testing and obviously is much larger in the range of c_i=16 to 41 MPa and φ_i=31 to 40° (tests were performed on similar rocks in the context of a dam project). The shear strength of the joints could not be measured in-situ, and was therefore estimated based on the Barton's empirical approach (Barton and Choubey, 1977). The shear strength of unfilled joints is influenced by the roughness, the strength of the joint surface and the normal stress acting on the discontinuity. On the basis of geometrical considerations and modelling results, it was assumed that the in-situ normal stresses acting on the basal shear zone were in the range between 4 to 18 MPa. According to the method of Barton and Choubey (1977) a friction angle ranging from 32° to 35°, by neglecting cohesion (c=0 MPa), was roughly estimated.

4.3 ~~4.3 Discontinuum~~ Distinct element modelling results

4.3.1 Modelling scenario I: initial deformation and failure mechanism of the rock slide

Model geometry, boundary conditions and material properties

As a basis, the SWW-NEE profile 2 (see Fig. 2 and 3) was chosen to study the initial deformation and failure mechanism based on the Universal Distinct Element Code (UDEC, Itasca 2020), by modelling both deformation and failure of blocks as well as shearing and opening of joints. As input the reconstructed pre-failure topography was taken to create the surface of the slope. Since this model type focuses on the initial formation mechanism of the rock slide the field-based and reconstructed basal shear zone was not included. However, the mapped structural anisotropy was considered by building a fractured rock mass

Formatiert: Mit Gliederung + Ebene: 2 + Nummerierungsformatvorlage: 1, 2, 3, … + Beginnen bei: 3 + Ausrichtung: Links + Ausgerichtet an: 0,63 cm + Einzug bei: 1,44 cm

Formatiert: Überschrift 3, Keine Aufzählungen oder Nummerierungen

Formatiert: Überschrift 4

model based on vertical and eastwards dipping joints (dip angle of 32°). Both joint sets are fully persistent and are spaced at 50 m. A finite difference mesh was calculated for deformable blocks by a zone edge-length of 10 m and a rounding length of 0.3 m. This avoids the problem of contact overlap, possibly resulting from the interaction of blocks occurring close to or at two opposing block corners (UDEC, Itasca 2020). A Mohr-Coulomb constitutive model was chosen from UDEC's plastic model group to simulate block deformation and failure. The failure envelope for this model corresponds to the Mohr-Coulomb criterion with a tension cut-off (tensile yield function). The shear flow rule is non-associated, and the tensile flow rule is associated (UDEC, Itasca 2020). Input requirements comprise as parameters the elastic bulk and shear modulus, the rock density, the cohesion and internal angle of friction, and in some cases the tension limit. For joints the Coulomb slip area contact model was taken to calculate shear displacement and slip. All selected physical, mechanical and hydraulic properties are summarized in Table 1.

No displacement boundaries were applied on the left, right and lower model boundary (Fig. 8a). The in-situ stresses were initialised in terms of a vertical gradient based on gravity and the horizontal stresses being half of the vertical stresses by assuming a k-ratio of 0.5. At the model origin (0,0) the two horizontal stresses were assigned to $\sigma_{xx}=\sigma_{zz}$ =25.6 MPa and the vertical stress to σ_{yy}=51.2 MPa, respectively. In models with groundwater flow a groundwater table was assumed with respect to characteristic groundwater flow patterns where the unsaturated zone between the surface and the water table is typically deep at the head of the slope, whereas the water table at the basis of the slope is close to or at the surface (Fig. 8a, e.g. Fetter 2001). For models calculating groundwater flow, the lower model boundary was set to no-flow (impermeable boundary). The left and right groundwater model boundaries were defined by a hydraulic gradient based on hydrostatic water pressure according to the assumed water table. The maximum water pressure was set to 19.72 MPa at the left boundary along the y-axis and to 8.96 MPa at the right boundary along the y-axis (Fig. 8a).

In order study the deformation and failure characteristics of the rock slope, selected block and joint parameters were varied. Concerning the elasto-plastic blocks cohesion was set to 0.1 and 1 MPa, internal friction angle to 20°, 25° and 30°, and tensile strength to 0 and 0.1 MPa. Joint cohesion and tensile strength was set to 0 MPa by varying the friction angle between 25°, 30° and 35° (Table 1). This model scenario focuses on intact block failure, its location and spatial arrangement, and the type of failure (i.e. tensile or shear failure) and provides insight into the general mechanisms of slope failure, formation of the rock slide geometry as well as into the initiation and progressive formation of a continuous basal shear zone.

Formatiert: Nicht Hervorheben

Formatiert: Nicht Hervorheben

Formatiert: Überschrift 4

Model scenario I - without groundwater flow

For this type of model runs a comprehensive parameter study was performed, by varying block plasticity and joint properties (see above and Table 1). In Figure 8a the spatial distribution of block displacement is shown, indicating a continuous decrease in magnitude from surface to depth, primarily caused by block deformation. It is also evident that localised line-shaped zones (e.g. several internal shear zones) were formed which suggest progressive fracturing and loosening of the rock mass, most likely penetrating from shallow to deeper domains (Fig. 8d). A comparison with the location of the mapped basal shear zone indicates that simulated slope deformations are not reaching deep-seated enough to reproduce the reconstructed slope situation

(i.e. location of the basal shear zone). However, the shape of the rock slide was adequately reproduced. By analysing the shear displacement of joints and shear failure pattern of blocks (Fig. 8d) in the rock mass, it was determined that a combination of structurally driven shear displacement and block failure was responsible for the observed slope deformation characteristics. Increased magnitudes of shear displacement were observed at the inclined joints in the middle and lower parts of the slope, reaching depths almost down to the location of the basal shear zone (Fig. 8c). In addition, large shear displacements were also observed near the summit on vertical joints, presumably induced by extensional stress regimes and rock mass subsidence. The pattern of block shear failure zones presented in Figure 8d clearly indicates the formation of several persistent shear zones, with failure processes occurring particularly frequently at the foot of the slope and in the summit area. Again, the deepest shear zone formed is too shallow and does not reach the location of the real shear zone, except at the foot of the slope. Results presented in Fig. 8b,c,d are based on the input parameters for blocks of c_b=0.1 MPa, and φ_b=30°, and for joints of c_j=0.1 MPa, and φ_j=25°. Changing the friction angle of the joints to 25° or 35°, respectively, while keeping the other parameters constant has no major impact on the modelling results. However, when varying the block friction angle to input values of 20°, 25°, 30°, 35° and 40°, where the block cohesion remains constant to c_b=0.1 MPa, the results obtained are different. Whereas, a block friction angle between 20° and 35° led to ongoing rock mass displacements reaching tens of metres, model runs with φ_b=40° stabilise after a few meters. Furthermore, the sensitivity of the model behaviour on varying block cohesion between 0.1 MPa and 1 MPa is expressed in strongly different displacement magnitudes, i.e. 50 m versus 1.7 m. In contrast, we have identified only a minor influence of block tensile strength on model behaviour. This is evident because tensile failure occurred primarily near the surface and at shallow depths (Fig. 8d).

Model scenario I - with groundwater flow

Model runs considering groundwater flow show similar results as dry models (Fig. 8). It has to be mentioned that due to UDEC's limitations, water pressure is only applied to joints, but not to blocks. A block friction angle of φ_b=30°, while c_b=0.1 MPa and the shear properties of the joints were set to c_j=0 MPa and φ_j=30°, caused a similar spatial distribution of block shear failure zones as observed under no ground water flow conditions (compare Fig. 8d and 8g). Multiple shear zones at different depths were also created in this model, an indication that intensive fracturing and loosening processes of the rock slide mass occurred. However, the simulation results did not confirm the hypothesis of a single basal shear zone located at the trace of reconstructed basal shear zone. Remarkably, the model run shown in Fig. 8g clearly indicates the formation of antithetic shear zones, i.e. structures which were often observed in the context of deep-seated rock slides and are appearing on surface as uphill facing scarps. Whereas block displacements of the previous model reached magnitudes of several decametres, increasing the block friction angle to φ_b=40°, while leaving the other parameters unchanged, reduced the overall displacement to less than 3.5 m. Even though, slope displacements were rather small, the simulation result suggests the initiation of a shear zone, mainly developing near the summit and less apparent near the foot. Nevertheless, the depth of the shear zone is clearly too small to be consistent with in-site observations.

Formatiert: Schriftart:

Formatiert: Schriftart: Kursiv, Tiefgestellt

Formatiert: Schriftart:

Formatiert: Schriftart: Nicht Fett

Formatiert: Schriftart: Nicht Fett, Deutsch (Österreich)

Formatiert: Schriftart: Nicht Fett

Formatiert: Schriftart: Nicht Fett, Kursiv

4.3.2 Modelling scenario II: back-calculation of shear strength properties of the basal shear zone

Model geometry, boundary conditions and material properties

Profile 2 (see Fig. 2 and 3) was taken for the back-calculation study based on distinct element modelling (UDEC, Itasca 2020) with a fully persistent basal failure zone. The pre-failure topography was implemented to create the surface of the slope, whilst the topography of the sliding surface provides the input for the basal shear zone (Fig. 9). The main deformation, i.e. shear and normal displacement, within the system takes place through the movement along the basal failure zone. Sliding and rotation of blocks, and opening and interlocking of interfaces i.e. joints make up the movement of the mass. In order to obtain numerical models that are manageable from the point of view of computer performance and computation time, the spacing of the joint sets was specified to 50 m in the rock slide mass and 150 m in the underlying granitic gneiss block (Fig. 9a and c). Two types of discontinuity networks were studied. The first type is characterised by a fully-persistent vertical and horizontal joint set, and the second type by a fully-persistent vertical and inclined joint set (dip angle of 32°), respectively. One reason to use a discontinuity geometry based on a vertical and horizontal fully persistent joint set was to have a good control over the groundwater flow conditions in the models, by achieving isotropic hydraulic conductivity. However, a structurally more realistic model geometry was added to this study. The finite difference mesh in the model was assigned by a size of 20 m in the rock slide mass and 50 m in the underlying granitic gneiss block. Rounding of block corners were applied with a radius of 0.3 m. The mechanical and hydraulic boundaries as well as the groundwater table were defined the same as in modelling scenario I (Fig. 9b,d). Blocks were considered as linear elastic defined by Hooke's law, considering components of stress to be linear functions of components of strain (Jaeger et al., 2007). Physical, mechanical and hydraulic properties used for the simulation are shown in Table 1. The Coulomb slip area contact model were assigned to the two joint sets and the basal shear zone. To investigate the impact of the discontinuity network on the back-calculated friction angle of the basal shear zone, the shear strength and tensile strength properties of the joints were varied (Table 1). The friction angle of the basal shear zone was varied between 20° and 28° for models without groundwater flow and between 25° and 32° considering groundwater flow. As an assumption, the cohesion of the basal shear zone was set c=0 MPa for all models. The determination of the critical angle of friction of the basal shear zone at failure was done by monitoring the maximum shear displacement along the basal shear zone, the block displacements (see monitoring points in Fig. 9a and c) and the unbalanced forces of the model, ideally reaching values close to zero.

Model scenario II - without groundwater flow

Concerning the model type without groundwater flow, the friction angles for the basal shear zone were varied between 20° and 31 whilst all other parameters were kept constant. However, to study also the impact of internal rock slide deformability the friction angle of the discontinuity network was set to 20, 30 and 40°. As a result, the back-calculated critical friction angles where failure was beginning was not a single value, but rather a range varying from 21 to 24°. In addition, it was found that a stepwise reduction of the friction angle led to increasing displacements, reaching nearly 6 m, associated with a re-stabilisation

Formatiert: Standard

Formatiert: Standard

Formatiert: Nicht Hervorheben

Formatiert: Nicht Hervorheben

Formatiert: Nicht Hervorheben

Formatiert: Nicht Hervorheben

Formatiert: Nicht Hervorheben

Formatiert: Schriftart: Nicht Fett

of the rock slide mass (Figs. 10a, b, c and d). Only a further reduction of the friction angle finally led to the progressing rock slide failure without stabilisation.

One major factor influencing the back-calculated critical friction angle was related to the shear strength properties of the joints in the rock slide mass by affecting the deformability (Fig. 11). On the one hand, a joint friction angle of φ_j=40° increases overall stability, which in turn requires a low friction angle of the basal shear zone values of φ_{bs}=21° to simulate failure. On the other hand, a rather low value of φ_j=20° assigned to the joints of the rock slide mass increase the critical friction angle of the basal shear to φ_{bs}=24°. A value in between, i.e. φ_j=30°, is resulting in a critical value of φ_{bs}=23° for the basal shear zone. Further, it was found that the influence of the discontinuity network orientation on slope deformation behaviour is rather small. Based on a joint friction angle of φ_j=40°, no difference in the displacement behaviour was observed between the model type with vertical and horizontal joints and the model type with vertical and inclined joints.

The magnitude and spatial distribution of shear displacement is affected by the shape of the basal shear zone (Figure 10b,d). Exemplarily, for the model types shown in Figure 10b and d (φ_j=30°, φ_{bs}=22°) the largest shear displacements were obtained in the upper part of the slope along the steepest section of the basal shear zone, reaching about 5.8 and 5.7 m. Towards the upper and lower sections of the shear zone, shear displacement continuously reduces to values of 3.75 m. The rock slide mass located above the steeply inclined section represents the domain which is most affected by internal deformation, i.e. due joint shearing (< 2 m) and opening (< 2 m) and thus clearly indicating the largest block displacements (Figure 10a and c). The shear to normal stress ratio (τ_s/σ_n) along the basal shear shows only minor fluctuations over the entire length of the shear zone, and the calculated τ_s/σ_n value is the range of the coefficient of friction (i.e. $\mu=tan(\varphi_{bs})$ applied to the model.

Model scenario II - with groundwater flow

The effect of groundwater flow due to ~~due~~ water pressure in the discontinuity network and basal shear zone on the back-calculated shear strength parameters was investigated for the two model types characterised by horizontally or inclined joint sets. In Figure 9b and d it is noticeable that the groundwater table performs a kink with steeper hydraulic gradient at the transition from the undeformed bedrock to the rock slide mass. Results showed a difference in the joint pressure distribution between the two geometric model types (Fig. 9b and d). Although, the same spacing and hydraulic aperture values were used the model with the inclined joint set resulted in lower water table accompanied by reduced joint water pressures. The reason for this can be found in the structural anisotropy changing the hydraulic conductivity from isotropic to anisotropic conditions. Similar to the model runs without groundwater flow (i.e. horizontal and vertical joint sets), the variation of the joint friction angle of the rock slide mass to values of 20, 30 and 40° influenced the back-calculated friction angle of the basal shear zone (Fig. 11). A joint friction angle of φ_j=40° results in a critical basal shear zone friction angle of φ_{bs}=27°. The reduction of the joint friction angle to φ_j=30° and φ_j=20° requires higher critical basal shear zone values of φ_{bs}=28°, and φ_{bs}=30°, respectively, to simulate failure. Depending on the possibility of shearing along joints the back-calculated friction angle of the basal shear zone varies between 28 and 31°. Interestingly, as opposed to the friction angle of the joints, the impact of tensile strength on the critical friction angle of the basal shear zone was minor. For example, changing the tensile strength to σ_z=1 MPa while

Formatiert: Standard

Formatiert: Tiefgestellt

Formatiert: Tiefgestellt

Formatiert: Schriftart:

Formatiert: Tiefgestellt

maintaining the joint friction angle to φ_j=40° showed nearly no effect on the back-calculated critical friction angle of the basal shear zone.

One major difference in comparison to the no groundwater flow models is related to the spatial distribution of shear displacement along the basal shear zone as well as overall rock slide displacement (Fig 10e and f). For model runs with horizontal and vertical joint sets shear displacement continuously increase from the foot of the slope to the scarp area, by reaching the largest values at the steepest section or in some cases above of it (Fig. 12). In contrast, the models assigned by an inclined joint set are indicating an opposing trend, with the largest shear displacements near the foot of the slope (Fig. 12). Geological structures influence the spatial distribution of shear displacement along the basal shear zone. Concerning the spatial distribution of rock slide displacements, a similar behaviour was observed from the simulations. Whereas the model runs with horizontal and vertical joints were yielding the largest displacements in the upper part of the rock slide, the opposite trend, with the maximum displacements at the foot of the slide, was observed for the model with inclined joints (Fig. 10e and f).

In summary, for model scenario II a critical friction angle ranging from 21 - 24° when no groundwater flow, and from 27 - 30° when groundwater flow was considered, was calculated.

Formatiert: Standard

Formatiert: Schriftart: Nicht Fett

Formatiert: Schriftart: Fett

~~**3.3.2 Model geometry, boundary and initial conditions**~~

~~Profile 2 (see Fig. 2 and 3) was taken for the discrete element (UDEC) modelling. The pre-failure topography was implemented to create the surface of the slope, whilst the topography of the sliding surface provides the input for the basal shear zone (Fig. 5). Blocks were considered as linear elastic defined by Hooke's law, considering components of stress to be linear functions of components of strain (Jaeger et al., 2007). The main deformation within the system takes place through the movement along discontinuities, i.e. shear and normal displacement. Sliding and rotation of blocks, and opening and interlocking of interfaces make up the movement of the mass (Itasca 2014).~~

~~Spacing of the joint set was assumed 50 m in the rock slide mass and 150 m in the underlying granitic gneiss block (see Fig. 5). The finite-difference mesh in the model was assigned by a size of 25 m in the rock slide mass and 50 m in the underlying granitic gneiss block. Rounding of block corners were applied with a radius of 0.5 m. This avoids the problem of contact overlap, possibly resulting from the interaction of blocks occurring close to or at two opposing block corners (Itasca 2014).~~

~~In the modelling scenario (B) a groundwater table was assumed with respect to characteristic groundwater flow patterns where the unsaturated zone between the surface and the water table is typically deep at the head of the slope, whereas the water table at the basis of the slope is close to or at the surface (see Fig. 5; e.g. Fetter 2001).~~

~~No displacement boundaries were applied on the left, right and lower model boundary (Fig. 5). For models with pore water pressure (B), the lower model boundary was set to a no-flow i.e. impermeable boundary. The left and right groundwater model boundary was defined by a hydraulic gradient based on hydrostatic water pressure according to the assumed water table. The maximum water pressure was set to 19.7 MPa at the left boundary along the y-axis and to 8.98 MPa at the right boundary along the y-axis (see Fig. 5). The in-situ stresses were initialised in terms of a vertical gradient based on gravity and the~~

horizontal stresses being half of the vertical stresses by assuming a k-ratio of 0.5. At the model origin (0,0) the two horizontal stresses were assigned to $\sigma_{xx} = \sigma_{zz} = 25.6$ MPa and the vertical stress to $\sigma_{yy} = 51.2$ MPa, respectively.

3.3.3 Material properties

The back-calculations of the friction angle of the basal shear zone were conducted with the assumption of the discontinuities of $\varphi = 30°$ (c=0 MPa) for the granitic gneiss of the failure mass and the underlying block (Table 1). The friction angle of the basal shear zone was varied between 20° and 27° for (A) and between 25° and 32° for (B), by assuming a cohesion of c=0 MPa. A density of $\rho = 2{,}600$ kg/m³ was assigned to all rock materials. Assuming a Young's modulus $E = 40$ GPa and a Poisson's ratio $\nu = 0.2$ a bulk modulus of 17 GPa and the shear modulus of 22 GPa of the granitic gneiss was obtained. Simplified conditions with a vertical and horizontal fully persistent joint set were implemented to simulate isotropic groundwater flow conditions for (B). Table 1 summarizes the material properties applied to the model.

4.3.1 Modelling results without pore water pressure (scenario A)

Values of $\varphi_{bs} = 20°$–$27°$ for the basal shear zone were varied for back-calculations in conditions without pore water pressure whilst all other parameters were kept constant. The determination of the critical angle of friction at failure was based on the obtained maximum shear displacement along the basal shear zone and the unbalanced forces of the model, ideally reaching values close to zero. As a result, the transition zone between stable conditions and failure was not a single value and found at approx. 24–25° (φ_{bs}; Fig. 9). Models with $\varphi_{bs} < 23.5°$ for the basal shear zone did not balanced to equilibrium, and thus indicating ongoing slope failure. Figure 10a shows the spatial distribution of displacement vectors of a model run reaching stabilisation ($\varphi_{bs} = 25°$). The maximum displacement values of about 0.25 m were reached at the top of the slope close to the peak. Lower values, ranging around 0.10 m, were reached in the lower part of the slope. The vectors of displacement increased again to values at around 0.25 m at the toe of the slope, indicating larger displacements there than in the middle of the slope. The values of the shear displacement along the basal shear zone were unequally distributed. The largest shear displacements were found at the top of the slope as well as at the slope toe, where the basal shear zone ends, with maximum values of around 0.24 m (see Fig. 10b). Smallest shear displacements were determined in the lower part reaching values below 0.12 m.

4.3.2 Modelling results with pore water pressure (scenario B)

The influence of pore water pressure on the behaviour of the slope was investigated by implementing a groundwater table to the model as defined in Section 3.3.2 (modelling scenario B). Results show that the model cannot be balanced with values of $\varphi_{bs} < 28°$ (see Fig. 9). In this case, the transition between stable conditions and failure was at approx. 28–29°. The transition between stable and unstable conditions were reflected in the sudden increase of the maximum shear displacement as shown in the graph in Fig. 9. Exemplarily, the friction angle of the basal shear zone is set to $\varphi_{bs} = 29°$ to further investigate the situation with pore water pressure. Maximum displacement values of approx. 1.80 m are found near the peak of the reconstructed mountain and decrease continuously with decreasing elevation, reaching a minimum of approx. 0.20 m at the toe of the slope (Fig. 11a). The maximum shear displacement along the basal shear zone reached a value of approx. 0.37 m (see Fig. 11b).

~~Shearing takes place at the basal shear zone as well as at vertical discontinuities in the upper part of the failing rock mass. The most pronounced shear displacement is predicted in the middle and lower part of the basal shear zone. As opposed to model run A, the middle to the upper part was characterised by minor shear displacements. Here, shearing along vertical discontinuities of around 0.15 m was computed near the topographic peak of the model.~~

5 Discussion

5.1 Reconstruction of rock slide topography, geometry, volume and sliding mass porosity

Topographic reconstructions, volumetric and porosity calculations of the failure and deposition mass of the Köfels Rock Slide have been made before by Brückl et al. (2001). They concluded from seismic data to physical properties of the rock mass. Based on an empirical relationship given by Watkins et al. (1972) the p-wave velocities were plotted versus depth to estimate the porosity of the deposition mass. On the basis of this calculation a relation between the thickness of the overburden and the porosity of the deposits was developed. The calculations by Brückl et al. (2001) resulted in a post-failure mean depth independent porosity of 23%. With an estimated failure volume of 3.28 km^3 and a deposition volume of 3.88 km^3, Brückl et al. (2001) calculated a volume increase of 18% due to disintegration, fracturing and loosening of the rock mass by the sliding process. The volume increase obtained by this study is 29% and therefore remarkably larger than obtained by Brückl et al. (2001). This discrepancy indicates that the computed volume increase is very sensitive to the computed failure and deposition volumes. Concerning the porosity of the deposition mass we calculated a value of 26%, a value similar to the 23% of Brückl et al. (2001).

5.2 Geomechanical modelling

In this study a topographic reconstruction was performed to provide a reasonable pre-failure, post-failure and geometrical model of the Köfels Rock Slide for subsequent numerical modelling. Given that slope inclination and rock slide geometry have a large impact on stability and limit-equilibrium, the detailed reconstruction of the pre-failure and post-failure slopes and the slide geometry done herein made possible comprehensive cross- and plausibility checks.

Distinct element modelling of the fractured rock slope rock without implementing a basal shear provides insight into the initial deformation and failure processes. Multiple shear zones at different depths were created in these models suggesting intensive fracturing and loosening of the rock slide mass during the initial phase of evolution, rather than forming a single basal shear zone. In addition, the formation of antithetic shear zones was observed during several model runs. Both features are typically for deep-seated rock slides and were frequently mapped either on surface as downhill or uphill-facing scarps, or explored in the subsurface by boreholes as shear zones composed of low-strength fault breccias and gouges (Rechberger et al. 2021, Strauhal et al. 2017). The formation of slabs is a further indicator for increased fracturing and loosening of the rock slide mass, and was determined on several case studies in crystalline rocks (Bonzanigo et al. 2007, Gluer et al. 2019, Zangerl et al. 2019). The obtained rock mass strength degradation process can be understood as the consequence of a complex interaction between

pre-existing joints and brittle fracture propagation through intact rock bridges, herein modelled as block failure. This modelling campaign does not take into account time-dependent processes and intact rock failure and crack propagation based on fracture mechanics. However, the simulation of zones of increased shear and tensile failure in blocks on the basis of a Mohr-Coulomb constitutive model can be assumed as progressive failure, at least to some extent. According to Eberhard et al. 2004 progressive failure in fractured rock slopes is related to the failure of individual rock bridges as their shear strength is exceeded. This in turn would increase the stresses ahead of the shear plane causing subsequent intact rock bridge failure in a consecutive manner, until the rupture surface extends to the point where kinematic release is possible. Although progressive failure must have played a crucial role in the genesis of the Köfels rock slides, additional factors must still have been involved to provide failure of such a strong rock mass.

The complex interaction of deformation and failure processes of blocks and joints, was investigated by a comprehensive parameter study, based on more than 50 different model runs. Large slope displacements associated with the formation of shear zones (i.e. block failures) were induced when the cohesion of the blocks is reduced to c_b=0.1 MPa and the internal friction angle to φ_b = 35°, by applying a friction angle of φ_j = 30° to the joint network. Increasing the internal friction angle of the blocks to c_b=1 MPa requires in turn a significant reduction in the friction angle to φ_b = 20° in order to simulate slope failure. In comparison, empirical estimations of the rock mass strength based on field surveys and the application of the GSI approach by Hoek and Brown (1997) show that the obtained shear strength values of the rock mass of c_{rm}=2 MPa and φ_{rm}=35° are too high to promote slope failure under static conditions.

The back-calculation of the shear strength of the basal shear zone based on UDEC (Itasca, 2020), assuming a cohesion of zero, in the present study results in values of $\varphi_{bs} \leq$ 21-24° without pore water pressure and $\varphi_{bs} \leq$ 27-30~~28~~° with pore water pressure. Consequently, given that the imposed boundary conditions, rock mass parameters and water pressure are valid, the friction angle of the ~~sliding surface~~basal shear zone may be constrained to the range φ_{bs} = 21~~4~~°–30~~28~~°. This very wide range results on the one hand from the influence of water pressure, and on the other hand from the internal deformability of the rock slide mass, primarily controlled by shearing along joints.

Brückl und Parotidis (2001) gained a value of the rock mass friction angle (φ_{rm}) between 20° and 24° from geomechanical continuum modelling of the Köfels Rock Slide. In a later approach, Brückl and Parotidis (2005) modelled the Köfels Rock Slide by applying a finite 2D-element method and focussing on modelling of the rock slide failure geometry. For their approach, they assumed a friction angle of φ_{bs} = 28°, without considering pore water pressure.

A preliminary comparison with 3D limit-equilibrium slope stability models (r.slope.stability; Mergili et al. 2013, 2014) indicates that the critical safety factors yielded by these models are within the range gained by the discontinuum approach, suggesting a certain degree of plausibility of the simulations ~~equal to 1 at approx. 1–3° higher values of φ, compared to the critical values derived in our discontinuum approach.~~ However, m~~M~~ore research is necessary to explore this issue, and particularly the influence of using 3D models.

~~The back-calculated friction angles of the basal shear zone required to induce slope failure are ranging from 24° to 28°. In comparison empirical estimations of the rock mass strength based on the GSI approach by Hoek and Brown (1997) show that~~

Kommentiert [c1]: Martin, das sollten wir nun nochmals überprüfen, da die Bandbreite nun von 21-30° reicht.

~~the obtained shear strength values of the rock mass of c_{rm}=2 MPa and φ_{rm}=35° are far too high to promote slope failure under static conditions.~~

Concerning unfilled and rough joints in granitic rocks the friction angle guessed by Barton and Choubey (1977) is several degrees higher than needed for slope failure. In-situ shear strength data for rough, unfilled joints in granitic rocks published by Fishmann (2004) show a remarkably high friction angle of φ_j=44° linked to a cohesion of c_j=0.08 and c_j=0.14 MPa, respectively. Grøneng et al. (2009) determined the shear strength of unfilled rock joints focusing on the Åknes rock slide in Norway by applying Barton-Bandis empirical equation. Applying their proposed parameters to an in-situ stress range from 4 to 18 MPa results in a friction angle between 31 and 36°. Grasselli (2001) performed shear tests on fresh tensile rock joints of gneisses and granites, additionally by applying up to 6 shear test cycles on the same samples. He measured values between 39° and 69° for the peak friction angle and values between 35° and 57° for the residual friction angle. Both, Byerlee (1978) and Hencher et al. (2011) determined a (basic) friction angle of around 40° for granitic rock joints.

In addition, field observations confirm that the fractures have a persistence in the scale of meters to tens of meters, and therefore it is assumed that the rock mass at the Köfels Rock Slides is characterised by intact rock bridges. It is widely accepted that intact rock bridges, if present, increase the shear strength of a rock mass (Jennings 1970, Einstein et al. 1983). Intact rock bridge failure is complex and usually not simply related to in-plane shear along the fractures, and is characterised by time-dependent progressive failure processes (sub-critical crack growth, Atkinson 1984, 1987). Nevertheless, conceptually and in the context of the Köfels Rock Slide intact rock bridges would further increase the overall rock mass strength of the slope, also when considering long-term conditions and the concept of progressive failure.

So far, the only possible geological discontinuity type which displays shear strength properties low enough to allow for slope failure under static conditions are pre-existing brittle fault zones composed with infillings of gouge and breccia. The parameters back-calculated by numerical modelling correspond reasonably well with the bandwidth of published values, ranging from 19° to 30°, observed for shear zones in crystalline rocks (Engl et al. 2008, Strauhal et al. 2017). However, our detailed geological field investigation and structural analyses of the high-resolution digital elevation models could indeed identify such structures in the rock mass, but not such ones which are dipping moderately towards east and are thus favourably aligned to promote the rock slide formation.

For example, an additional geological factors reducing the rock mass strength by rock mass fracturing and weakening of large rock slopes to depths of several hundred metres is related to deep-seated block or flexural toppling processes (Amann 2006, Casson et al. 2003, Zangerl et al. 2015). Deep-seated toppling occurs when steeply inclined structures are present and this failure mechanism is often observed in foliated metamorphic rock mass with low to moderate strengths (paragneisses, schists and phyllites). However less common, but still observed is toppling in granitic gneisses when foliation as well as joint planes and fault zones are closely spaced and steeply dipping into the slope (Amann 2006). Structural mapping by Prager et al. (2010) and this study in the surrounding of the scarp confirm steeply dipping NNW-SSE striking joints and faults. Though structurally possible, it is questionable if deep-seated toppling is a preparatory mechanism for the Köfels rock mass failure, because no clear geomorphological and structural indicators for toppling were found in the surrounding of the scarp.

Based on the results of the numerical modelling study it is inconceivable that slope failure occurred under pure static conditions, even when a high groundwater table, causing extraordinary high pore pressures, is assumed. Apart from that permafrost degradation due to climate warming has often been discussed as a relevant factor for slope failure in rock masses. So far it is widely accepted that permafrost degradation can alter the rock mass strength by ice melting and temperature changes (Dramis et al. 1995, Fischer et al. 2006, Huggel et al. 2012, Krautblatter et al. 2013). According to the time-depended rock-ice mechanical model proposed by Krautblatter et al. 2013 it is assumed that ice-rock mechanical processes are more relevant for rock slope failures at shallow depths (less than 20 m) whereas rock-rock mechanical processes are dominating at greater depth. Considering this geomechanical concept in relationship to the great depth of the rupture surface of several hundred metres, as well as the time lag of two millennia between Holocene warming and slope failure (Nicolussi et al. 2015), permafrost degradation acting as major trigger of the Köfels rock slide is unlikely. Based on the findings of this study, climate-driven triggering factors characterised by periods of increased precipitation rates or permafrost degradation were probably too weak to provoke such a large-scale slope failure.

One interesting observation was done by Nicolussi et al. 2015 who performed precise age-dating of the 3.1 km^3 large Köfels rock slide based on tree-ring analysis and radiocarbon dating, constraining the event to 9527–9498 cal BP. Remarkably, the new age bandwidth is close to the age of the Flims landslide ranging from 9480–9430 cal BP, the largest rock slide in the Alps, comprising a volume of 8–12 km^3 (Poschinger and Kippel 2009). Furthermore, a few more events occurring in the eastern alps show ages clustering within this period (Prager et al. 2008, Borgatti and Soldati 2010). The close temporal and spatial relationship between the Köfels and Flims rock rlide raises the question whether dynamic loading due to earthquake shaking was able to trigger two of the largest rock slides in the Alps, located only about 130 km apart. Oswald et al. 2021 concluded from high-resolution lacustrine paleoseismology a relation between past seismicity and a spatio-temporal cluster of large prehistoric rock slides in the Eastern Alps, e.g. the Eibsee, Fernpass, and Tschirgant Rock Slides (Prager et al. 2008). They also found that the Köfels Rock Slide was not directly earthquake-triggered, but failed some centuries later after at least one severe earthquake around 9.9 ka BP. Kremer et al. 2020 proposed an enhanced seismic activity in the Alps in the period 9.5 – 9.9 ka BP. Based on the chronology of earthquake events during the Holocene, Oswald et al. 2021 assume that earthquakes are more important for preparing rock slopes towards failure due to seismic fatigue than for being the ultimate trigger. In the context of this numerical modelling study progressive failure reinforced by seismic fatigue can explain to some extent the discrepancy between the rock mass strength estimated from rock mechanical assessment and those obtained by back-calculation. However, seismic fatigue cannot solely explain the particular situation of the Köfels Rock Slide, because it is still unclear why this giant event occurred at this location, and in a very strong rock mass. With regard to the surrounding area, the reconstructed pre-failure slope is neither particularly steep nor characterized by other eye-catching features. However, it is assumed that beside the other factors a special geological predisposition (e.g. favorably orientated and very high persistent discontinuities) may have contributed to lead to the occurrence of the event.

~~The close temporal relationship of failure between the Köfels and Flims Rock Slide raises the question whether dynamic loading due to earthquake shaking was able to trigger two of the largest rock slides in the Alps, located about 130 km apart.~~

~~Up to now it could not be proven if a high magnitude earthquake has been happened at this time (palaeo seismic records are incomplete). Furthermore, it is not clear how strong the earthquake must have been and whether this hypothesis can be in accordance with seismo tectonic considerations of the Alps. Conceptually, it would be expected that a large earthquake triggering these two extremely large rock slides would have caused numerous (smaller) events, dating with the same age with failure locations somewhere in between. Thus, we suggest further investigations comprising palaeo seismic analyses, age-dating, geotechnical shear testing of material from ruptures surfaces, and dynamic numerical modelling efforts in order to shed light on these aspects.~~

6. Conclusions

Based on geologic, geophysical and topographic constraints, we reconstructed three topographic stages of the Köfels Rock Slide: i) the pre-failure topography with the reconstructed mountain ~~peak~~summit, ii) the topography demonstrating the sliding surface without rock slide deposit, iii) the post-failure topography with the deposits in the valley but before their incision by the river Ötztaler Ache. For the failure volume a value of 3.1 km³ is gained, the deposition volume is calculated as about 4.0 km³. These values are very close to those derived by Brückl et al. (2001), leading to the conclusion that the estimates gained of the volumes are sufficiently robust.

Knowledge on the volume increase of the rock mass during sliding is less robust, as the derived values react very sensitive even to small variations in the failure and deposition volumes. Whilst Brückl et al. (2001) come to an increase in volume by 18%, our study suggests an increase by 29%. The porosity of the failed rock slide mass increased to a mean of 26%, with wide variations.

Based on distinct element models by varying the block and joint input parameters the deformation and failure process of the rock slope could be plausibly reconstructed, however, the exact geometry of the rock slide, especially in view of thickness, could not be fully reproduced. Our results suggest that both failure of rock blocks and shearing along moderately eastward dipping joints were responsible for the formation or the rock slide. The progressive failure process may have taken place by fracturing, fragmentation and loosening of the rock mass, advancing from shallow to deeper zones of the slope. The progressive rock mass degradation led to the formation of multiple shear zones at different depths and antithetic structures such as uphill facing scarps.

The shear strength of the basal shear zone at failure in conditions without and with pore water pressure is back-calculated by the ~~two-dimensional~~ distinct element ~~code UDEC~~method. The back-calculation study is based on the assumption of a continuous basal shear zone derived from field mapping and high resolution digital elevation models and a cohesion of zero, resulting in values of $\varphi_{bs} \leq$ 21-24° without pore water pressure and $\varphi_{bs} \leq$ 27-30~~28~~° with pore water pressure. However, field

observations suggest that a continuous basal shear zone may have formed during the initial failure stage of the slide, but there is no evidence for a pre-existing zone of weakness promoting slope failure. Comparisons of back-calculated shear strength of the basal shear zone with values roughly assessed for the fractured granitic rock mass show that slope failure under static conditions is unlikely, even under high pore pressures. In addition to a particular geological disposition, increased seismic activity over a longer period of time is believed to have been a major driver of the progressive strength degradation process responsible for the rapid failure of the Köfels Rock Slide. ~~Additional triggering factors, for example impact of dynamic loading have to be considered in further investigations.~~

Acknowledgements

This study was part of the alpS research projects 'ProMM' and 'AdaptInfra', which were supported by TIWAG, geo.zt, ILF Consulting Engineers and the Austrian Research Promotion Agency (COMET-program). The alpS-K1-Centre was supported by Federal Ministries BMVIT and BMWFW as well as the States of Tyrol and Vorarlberg in the framework of "COMET-Competence Centers for Excellent Technologies". COMET is processed through FFG.

References

Abele, G.: Large rockslides: their causes and movements on internal sliding planes. Mt Res Dev 14:315–320, DOI: 10.2307/3673727, 1994.

Amann, F.: Großhangbewegung Cuolm da Vi (Graubünden, Schweiz). Geologisch-geotechnische Befunde und numerische Untersuchungen zur Klärung des Phänomens. Dissertation, Friedrich-Alexander Universität Erlangen-Nürnberg, p. 206, 2006.

Ampferer, O.: Über die geologischen Deutungen und Bausondierungen des Maurach Riegels im Ötztal. Geologie und Bauwesen 11:25–43, 1939.

Ascher, H.: Neuer Sachbestand und Erkenntnisse über das Bergsturzgebiet von Köfels. Geologie und Bauwesen 19:128–134, 1952.

Atkinson, B.K.: Subcritical crack growth in geological materials. Journal of Geophysical Research 89 (B6): 4077-4114, https://doi.org/10.1029/JB089iB06p04077, 1984.

Atkinson, B.K.: Introduction to fracture mechanics and its geophysical applications. In: Atkinson BK (ed), Fracture mechanics of rock, Academic Press, 1-26, 1987.

Borgatti, L. and Soldati, M.: Landslides as a geomorphological proxy for climate change: a record from the Dolomites (northern Italy). Geomorphology 120, 56–64, https://doi.org/10.1016/j.geomorph.2009.09.015, 2010.

Brückl, E. and Parotidis, M.: Estimation of large-scale mechanical properties of a large landslide on the basis of seismic results. Rock Mech Min Sci 38:877–883, https://doi.org/10.1016/S1365-1609(01)00053-3, 2001.

Brückl, E. and Parotidis, M.: Prediction of slope instabilities due to deep-seated gravitational creep. Nat Hazards Earth Syst Sci 5:155–172, 2005.

Brückl, E. and Heuberger, H.: Reflexionsseismische Messungen am Bergsturz von Köfels. Geologie des Oberinntaler Raumes – Schwerpunkt Blatt 144 Landeck:156–158. Geologische Bundesanstalt, Vienna, 1993.

Brückl, E., Brückl, J. and Heuberger, H.: Present structure and prefailure topography of the giant rockslide of Köfels. Zeitschrift für Gletscherkunde und Glazialgeologie 37(1):49–79, https://doi.org/10.3997/2214-4609.201407174, 2001.

Brückl, E., Brückl, J., Chwatal, W. and Ullrich, C.: Deep alpine valleys: examples of geophysical explorations in Austria. Swiss J Geosci 103:329–344, https://doi.org/10.1007/s00015-010-0045-x, 2010.

Bonzanigo, L., Eberhardt, E., Loew, S.: Long-term investigation of a deep-seated creeping landslide in crystalline rock. Part I. Geological and hydromechanical factors controlling the Campo Vallemaggia landslide. Can. Geotech. J. 44, 1157–1180. https://doi.org/10.1139/T07-043, 2007.

Byerlee, J.: Friction of rocks. Pure Appl Geophys 116:615–626, https://doi.org/10.1007/978-3-0348-7182-2_4, 1978.

Casson, B., Delacourt, C., Baratoux, D. and Allemand, P.: Seventeen years of the ‘‘La Clapière’’ landslide evolution analysed from ortho-rectified aeri-al photographs. Engineering Geology 68: 123-139, https://doi.org/10.1016/S0013-7952(02)00201-6, 2003.

Dai, F.C., Lee, C.F. and Yip Ngai, Y.: Landslide risk assessment and management: an overview. Engineering Geology 64(1):65–87, https://doi.org/10.1016/S0013-7952(01)00093-X, 2002.

Eberhardt, E., Stead, D., Coggan, J.S.: Numerical analysis of initiation and progressive failure in natural rock slopes-the 1991 Randa rockslide. Int. J. Rock Mech. Min. Sci. 41, 69–87. https://doi.org/10.1016/S1365-1609(03)00076-5, 2004.

Einstein, H.H., Veneziano, D., Baecher, G.B. and O'Reilly, K.J.: The Effect of Discontinuity Persistence on Rock Slope Stability. International Journal of Rock Mechanics and Mining Sciences, Vol. 20, No. 5, pp. 227-236, https://doi.org/10.1016/0148-9062(83)90003-7, 1983.

Engl, D.A., Fellin, W. and Zangerl, C.: Scherfestigkeiten von Scherzonen-Gesteinen – Ein Beitrag zur geotechnischen Bewertung von tektonischen Störungen und Gleitzonen von Massenbewegungen. Bulletin für Angewandte Geologie 13(2):63–81, 2008.

Erismann, T.H. and Abele, G.: Dynamics of Rockslides and Rockfalls. Springer, Berlin, 2001.

Erismann, T.H., Heuberger, H. and Preuss, E.: Der Bimsstein von Köfels (Tirol), ein Bergsturz-"Friktionit". Tschermaks Mineralogische und Petrographische Mitteilungen 24:67–119, https://doi.org/10.1007/BF01081746, 1977.

Evans, S.G., Bishop, N.F., Fidel Smoll, L., Valderrama Murillo, P., Delaney, K.P. and Oliver-Smith, A.: A re-examination of the mechanism and human impact of catastrophic mass flows originating on Ne-vado Huascarán, Cordillera Blanca, Peru in 1962 and 1970. Engineering Geology 108:96–118, https://doi.org/10.1016/j.enggeo.2009.06.020, 2009a.

Evans, S.G., Roberts, N.J., Ischuk, A., Delaney, K.B., Morozova, G.S. and Tutubalina, O.: Landslides triggered by the 1949 Khait earthquake, Tajikistan, and associated loss of life. Engineering Geology 109:195–212, https://doi.org/10.1016/j.enggeo.2009.08.007, 2009b.

Evans, S.G. and DeGraff, J.V.: Catastrophic landslides: Effects, occurrence, and mechanism. Geol Soc Am Rev Eng Geol 15, 2002.

Fetter, C.W.: Applied Hydrogeology. Vol. 4. Prentice Hall Inc., New Jersey, 2001.

Fischer, L., Kääb, A., Huggel, C., Noetzli, J.: Geology, glacier retreat and permafrost degradation as controlling factors of slope instabilities in a high-mountain rock wall: the Monte Rosa east face Nat. Hazards Earth Syst. Sci., 6, 761–772, https://doi.org/10.5194/nhess-6-761-2006, 2006.

Genevois, R. and Ghirotti, M.: The 1963 Vaiont Landslide. Giornale di Geologia Applicata 1:41–52, doi: 10.1474/GGA.2005-01.0-05.0005, 2005.

Glüer, F., Loew, S., Manconi, A., Aaron, J.: From toppling to sliding: progressive evolution of the Moosfluh Landslide. Switzerland. JGR Earth Surf. 124 (12), 2899–2919. https://doi.org/10.1029/2019JF005019, 2019.

Govi. M, Gullà, G. and Nicoletti, P.G.: Val Pola rock avalanche of July 28, 1987, in Valtellina (Central Italian Alps). In: Evans SG, DeGraff JV (eds) Catastrophic landslides: Effects, occurrence, and mechanism. Geol Soc Am Rev Eng Geol 15:71–89, 2002.

Hencher, S.R., Lee, S.G., Carter, T.G. and Richards, L.R.: Sheeting Joints: Characterisation, Shear Strength and Engineering. Rock Mech Rock Eng (2011) 44:1–22, https://doi.org/10.1007/s00603-010-0100-y, 2011.

Heuberger, H. The giant landslide of Köfels, Ötztal, Tyrol. Mount Res Dev 13(4):290–294, 1994.

Huggel, C., Clague, J.J. and Korup, O.: Is climate change responsible for changing landslide activity in high mountains? Earth Surf. Process. Landforms 37, 77–91, https://doi.org/10.1002/esp.2223, 2012.

Itasca: UDEC - Universal distinct element code, Version 7~~6~~.0. Minneapolis, Itasca ConsultingGroup, 2020~~14~~.

Ivy-Ochs, S., Heuberger, H., Kubik, P.W., Kerschner, H., Bonani, G., Frank, M., Schlüchter, C.: The age of the Köfels event. Relative, 14C and cosmogenic isotope dating of an early holocene landslide in the central alps (Tyrol, Austria). Zeitschrift für Gletscherkunde und Glazialgeologie 34:57–68, 1998.

Jaeger, J.C., Cook, N.G.W. and Zimmermann, R.W.: Fundamentals of Rock Mechanics. Vol. 4. Blackwell Publishing, Malden, Mass, 2007.

Jennings, J.E.: A Mathematical Theory forthe Calculation ofthe Stability of Open Case Mines. Proc. Symp. on the Theoretical Background to the Planning of Open Pit Mines. pp. 87-102, Johannesburg, 1970.

Kilburn, C.R.J. and Pasuto, A.: Major risks from rapid, large-volume landslides in Europe (EU Project RUNOUT). Geomorphology 54:3–9, https://doi.org/10.1016/S0169-555X(03)00050-3, 2003.

Krautblatter, M., Funk, D., and Günzel, F.K.: Why permafrost rocks become unstable: A rock-ice-mechanical model in time and space. Earth Surf. Process. Landforms 38:876–887, https://doi.org/10.1002/esp.3374, 2013.

Kremer, K., Gassner-Stamm, G., Grolimund, R., Wirth, S.B., Strasser, M., Fäh, D.: A database of potential paleoseismic evidence in Switzerland. J. Seismol. 24, 247–262, https://doi.org/10.1007/s10950-020-09908-5, 2020.

Kubik, P.W., Ivy-Ochs, S., Masari, J., Frank, M. and Schlüchter, C.: 10Be and 26Al production rates deduced from an instantaneous event within the dendro-calibration curve, the landslide of Köfels, Ötz Valley, Austria. Earth Planet Sci Lett 161:231–241, https://doi.org/10.1016/S0012-821X(98)00153-8, 1998.

Kveldsvik, V., Kaynia, A.M., Nadim, F., Bhasin, R., Nilsen, B. and Einstein H.H.: Dynamic distinct-element analysis of the 800 m high Aknes rock slope. Int J Rock Mech Min Sci 46(4):686–698, https://doi.org/10.1016/j.ijrmms.2008.10.007, 2009.

Margottini, C., Canuti, P. and Sassa, K.: Landslide Science and Practice. 7 volumes. Springer, Berlin, Heidelberg, 2013.

Mergili, M., Marchesini, I., Rossi, M., Guzzetti, F. and Fellin, W.: Spatially distributed three-dimensional slope stability modelling in a raster GIS. Geomorphology 206:178–195, https://doi.org/10.1016/j.geomorph.2013.10.008, 2014.

Mergili, M., Marchesini, I., Alvioli, M., Metz, M., Schneider-Muntau, B., Rossi, M. and Guzzetti, F.: A strategy for GIS-based 3-D slope stability modelling over large areas. Geosci Model Dev Disc 7:5407–5445, doi:10.5194/gmd-7-2969-2014, 2014.

Milton, D.J.: Fused rock from Köfels, Tyrol. Tschermaks mineralogische und petrographische Mitteilungen 9:86–94, https://doi.org/10.1007/BF01127777, 1964.

Nadim, F., Kjekstad, O., Peduzzi, P., Herold, C. and Jaedicke C.: Global landslide and avalanche hotspots. Landslides 3(2):159–173, https://doi.org/10.1007/s10346-006-0036-1, 2006.

Nicolussi, K., Spötl, C., Thurner, A., Reimer, P.J.: Precise radiocarbon dating of the giant Köfels landslide (Eastern Alps, Austria), Geomorphology, Volume 243, Pages 87-91, https://doi.org/10.1016/j.geomorph.2015.05.001, 2015.

Pichler, A.: Zur Geognosie Tirols II. Die vulkanischen Reste von Köfels. Jahrbuch der Geologischen Reichsanstalt in Wien 13:591–594, 1863.

Oswald, P., Strasser, M., Hammerl, C. and Moernaut, J.: Seismic control of large prehistoric rockslides in the Eastern Alps. Nature Communications, 12(1): 1059, https://doi.org/10.1038/s41467-021-21327-9, 2021.

Pirkl, H.R.: Die westlichen Zentralalpen (von der Silvretta zum Brenner). In: Oberhauser R, and geologische Bundesanstalt (eds) Der geologische Aufbau Österreichs:332–347. Springer, Vienna, New York, 1980.

Poschinger, A. and Kippel, T.: Alluvial deposits liquefied by the Flims rock slide. Geomorphology 103 (2009) 50–56, https://doi.org/10.1016/j.geomorph.2007.09.016, 2009.

Prager, C., Zangerl, C., Patzelt, G. and Brandner, R.: Age distribution of fossil landslides in the Tyrol (Austria) and its surrounding areas. Nat. Hazards Earth Syst. Sci. 8, 377–407, https://doi.org/10.5194/nhess-8-377-2008, 2008.

Prager, C., Zangerl, C. and Nagler, T.: Geological controls on slope deformations in the Köfels rockslide area (Tyrol, Austria). Austrian J Earth Sci 102(2):4–19, 2009.

Preuss, E., Masch, L. and Erismann, T.H.: Friktionite - Natürliches Glas aus der Reibungsschmelze sehr großer Bergstürze (Köfels, Tirol - Langtang, Nepal). Proceedings of the 2nd International Conference on Natural Glasses, Prague:1–4. Charles University, Prague, 1987.

Formatiert: Unterstrichen

Preuss, E.: Der Bimsstein von Köfels im Ötztal/Tirol – Die Reibungsschmelze eines Bergsturzes. Vol. 39. Verein zum Schutze der Alpenpflanzen und -Tiere, Munich, 1974.

Preuss, E.: Gleitflächen und neue Friktionitfunde im Bergsturz von Köfels im Ötztal, Tirol. Material und Technik – Schweizerische Zeitschrift für Werkstoffe, Betriebsstoffe, Materialprüfung und Messtechnik 3. Schweizerischer Verband für die Materialprüfung der Technik (SVMT), 1986.

Purtscheller. F., Pirchl, T., Sieder, G., Stingl, V., Tessadri, T., Brunner, P., Ennemoser, O. and Schneider, P.: Radon emanations from giant landslides of Koefels (Tyrol, Austria) and Langtang Himal (Nepal). Environ Geol 26: 32–38, https://doi.org/10.1007/BF00776029, 1995.

Rechberger, C., Fey, C., Zangerl, C.: Structural characterisation, internal deformation, and kinematics of an active deep-seated rock slide in a valley glacier retreat area. Engineering Geology 286, https://doi.org/10.1016/j.enggeo.2021.106048, 2021.

Sassa, K., Canuti, P., and Yin, Y.: Landslide Science for a Safer Geoenvironment. 3 volumes. Springer, Cham, Heidelberg, New York, Dordrecht, London, 2014.

Sørensen, S.A. and Bauer B.: On the dynamics of the Köfels sturzstrom. Geomorpholgy 54:11– 19, https://doi.org/10.1016/S0169-555X(03)00051-5, 2003.

Strauhal, T., Zangerl, C., Fellin, W., Holzmann, M., Engl, D.A., Brandner, R., Tropper, P., Tessadri, R.: Structure, mineralogy and geomechanical properties of shear zones of deep-seated rockslides in metamorphic rocks (Tyrol, Austria). Rock Mech. Rock. Eng. 50 (2), 419–438. https://doi.org/10.1007/s00603-016-1113-y, 2017.

Stutzer, O.: Die Talweitung von Köfels im Ötztal (Tirol) als Meteorkrater. Zeitschrift der Deutschen Geologischen Gesellschaft 88:523–525, 1936.

Suess, F.E.: Der Meteor-Krater von Köfels beim Umhausen im Ötztale, Tirol. Neues Jahrbuch für Mineralogie, Geologie und Paläontologie, Abh., 72:98–155, 1937.

von Klebelsberg, R.: Das Becken von Längenfeld im Ötztal. Ein Beispiel für Geologie und Kraftwerksplanung. Schlern-Schriften 77:399–422, 1951.

von Klebelsberg, R.: Geologie von Tirol. Gebrüder Borntraeger, Berlin, 1935.

von Poschinger, A.: Large rockslides in the Alps: A commentary on the contribution of G. Abele (1937-1994) and a review of some recent developments. In: Evans SG, DeGraff JV (eds), Catastrophic Landslides: Effects, Occurence, and Mechanisms. Geol Soc Am Rev Eng Geol 15:237–257, 2002.

Weidinger, J.T.: Predesign, failure and displacement mechanisms of large rockslides in the Annapurna Himalayas, Nepal. Engineering Geology 83: 201–216, https://doi.org/10.1016/j.enggeo.2005.06.032, 2006.

Weidinger, J.T., Korup, O., Munack, H., Altenberger, U., Dunning, S.A., Tippelt, G. and Lottermoser, W.: Giant rockslides from the inside. Earth Planet Sci Lett 389:62–73, https://doi.org/10.1016/j.epsl.2013.12.017, 2014.

Zangerl C, Eberhardt E, Evans KF, Loew S (2003) Analysis of Subsurface Subsidence in Crystalline Rock above the Gotthard Highway Tunnel, Switzerland. Swiss Federal Institute of Technology (ETH), Zurich.

Zangerl, C., Chwatal, W. and Kirschner, H.: Formation processes, geomechanical characterisation and buttressing effects at the toe of deep-seated rock slides in foliated metamorphic rock. Geomorphology. 243: 51-64, https://doi.org/10.1016/j.geomorph.2015.03.030, 2015.

Zangerl, C., Fey, C., Prager, C.: Deformation characteristics and multi-slab formation of a deep-seated rock slide in a high alpine environment (Bliggspitze, Austria). Bull. Eng. Geol. Environ. 78, 6111–6130. https://doi.org/10.1007/s10064-019-01516-z, 2019.

Figures

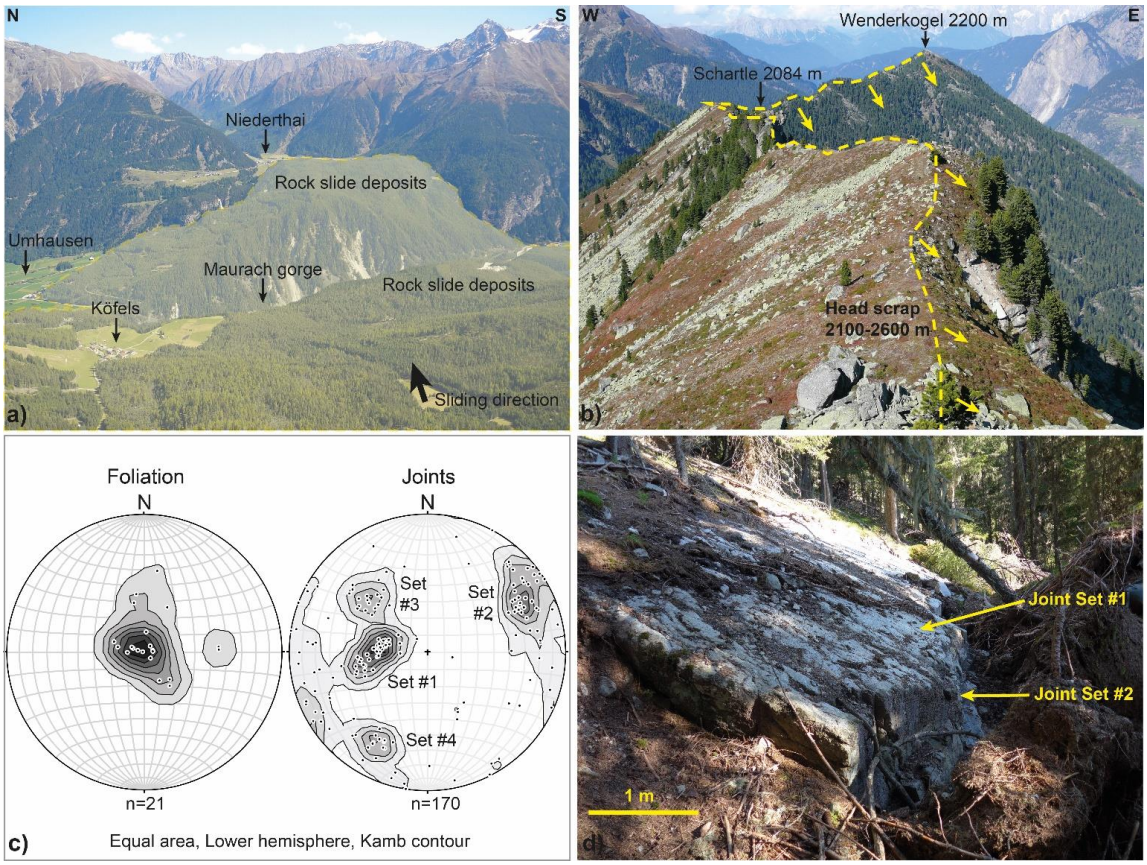

Figure 1. a) Panoramic view of the Köfels Rock Slide deposits from head scarp towards E with the Maurach Gorge cutting through the deposits (centre) and the backwater sediments in Niederthai (right), b) View of the head scarp from S to N, c) Measured foliation and joint planes (poles to planes) in the surroundings of the central part of the head scarp, and d) outcropping rupture surface formed along a moderately dipping plane of joint set #1 and linked with joint set #2 (stepped failure plane).

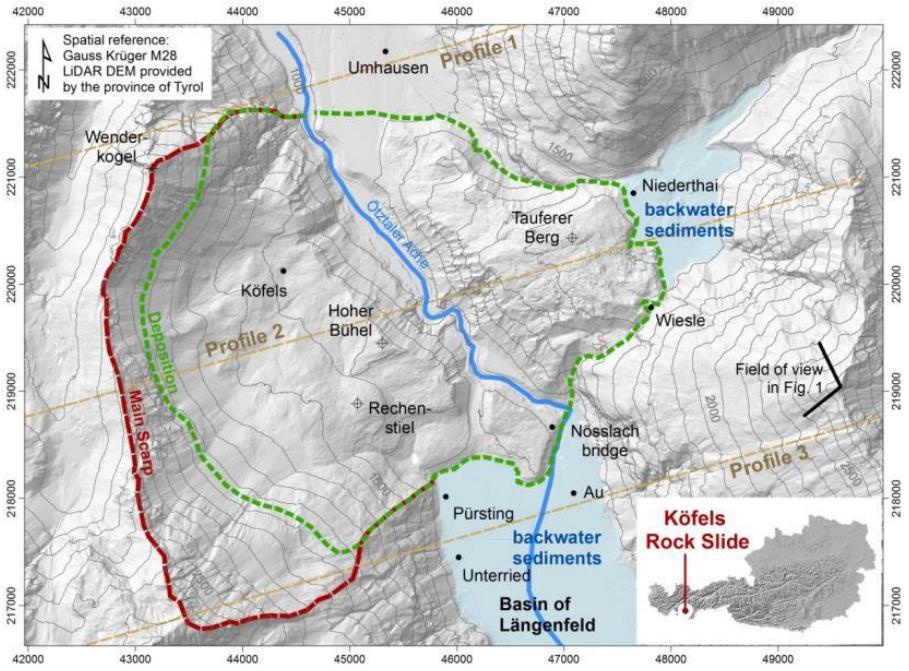

Figure 2: Overview map of the Köfels Rock Slide area.

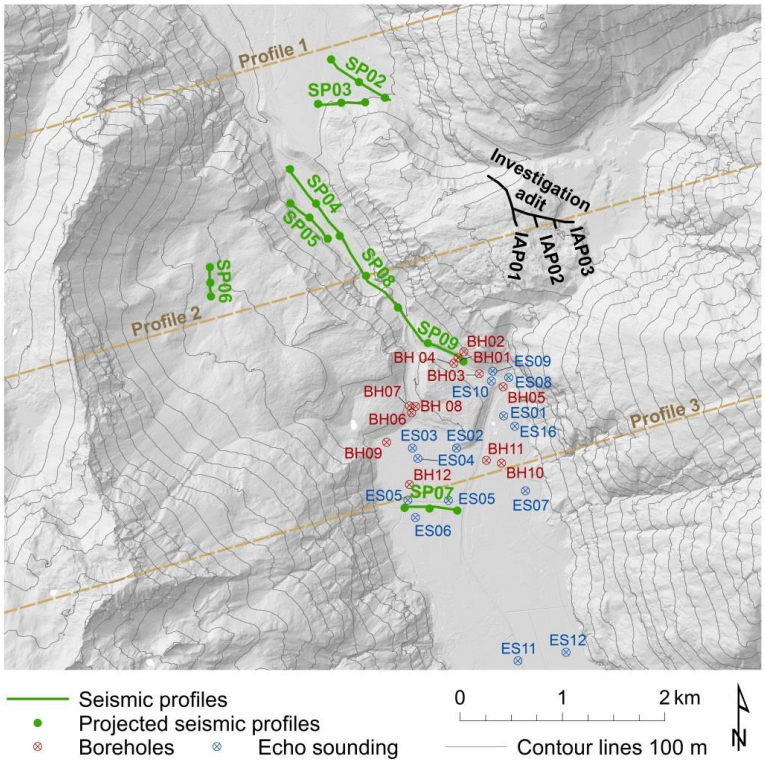

Figure 3: Borehole data (BH), echo-sounding (ES) and seismic profiles (SP) used for the topographic reconstruction of the Köfels Rock Slide.

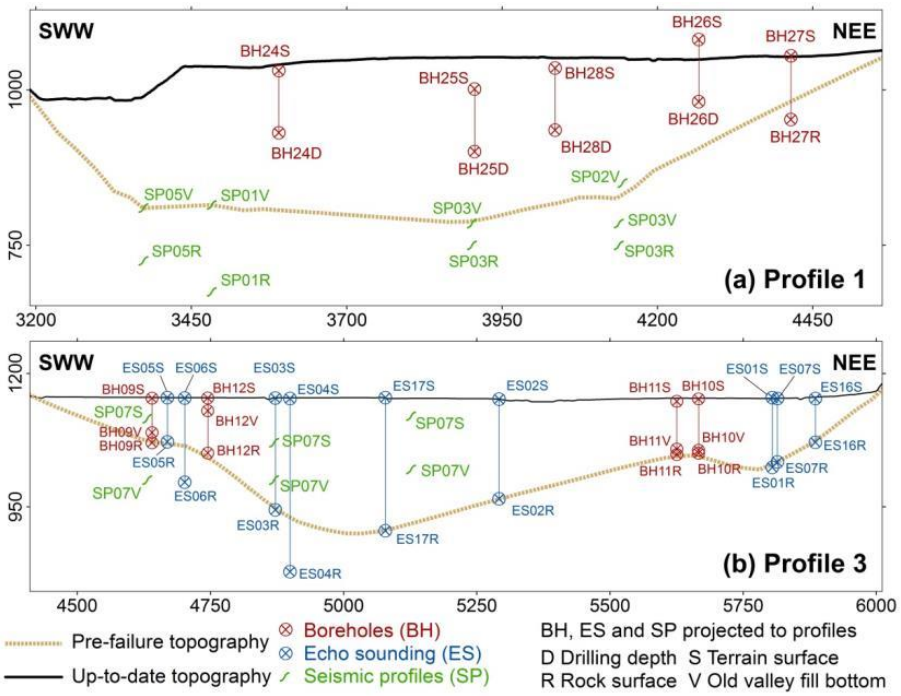

Figure 4: Profiles through the valley bottom in the Köfels Rock Slide area (see Figs. 2 and 3). (a) Profile 1 in the north of the Köfels site, basin of Umhausen. (b) Profile 3 in the south of the Köfels site, basin of Längenfeld. Note that the point data and seismic profiles (see Fig. 3) are projected to the profile planes and therefore do not necessarily correspond to the topographic surfaces shown.

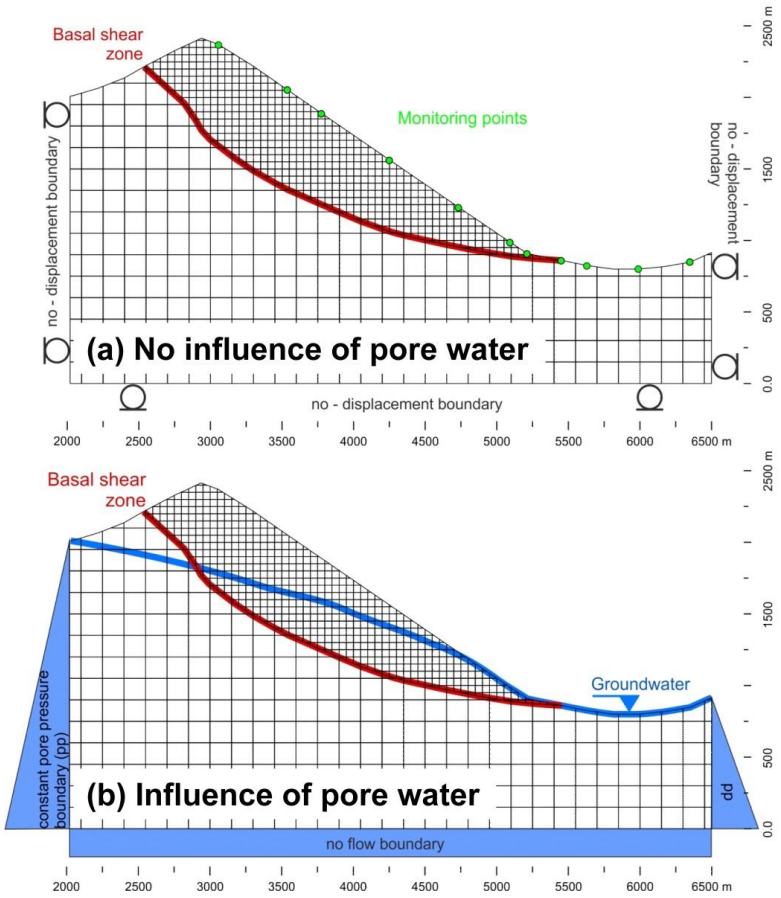

~~Figure 5: Model geometry with boundary conditions, joint sets for the failure rock mass and the underlying rock mass. (a) shows the monitoring points where deformations are recorded. (b) shows the groundwater table applied to the modelling scenario (B) assuming the typical trend of groundwater flow in slopes.~~

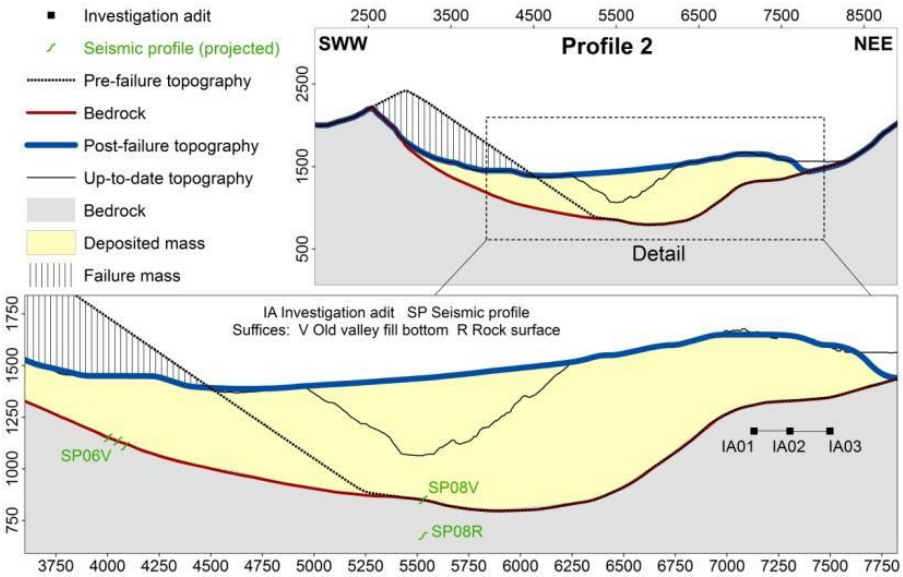

Figure 5~~6~~: Profile 2 (see Figs. 2 and 3) through the Köfels site with the three reconstructed stages and the up-to-date topography.

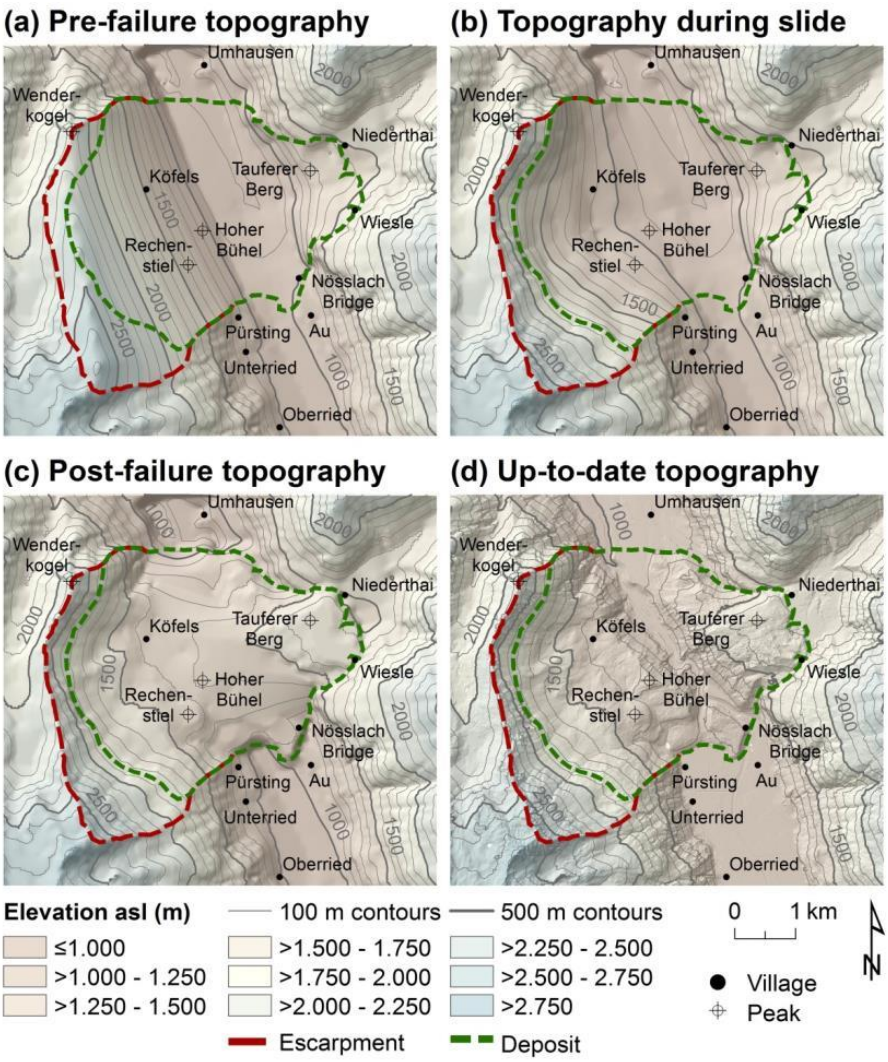

Figure 6~~7~~: DEM of the three reconstructed stages and the up-to-date topography. (a) pre-failure, (b) bedrock, (c) post-failure, (d) up-to-date. The spatial resolution of the DEMs is 30 m in (a)–(c) and 1 m in (d).

950

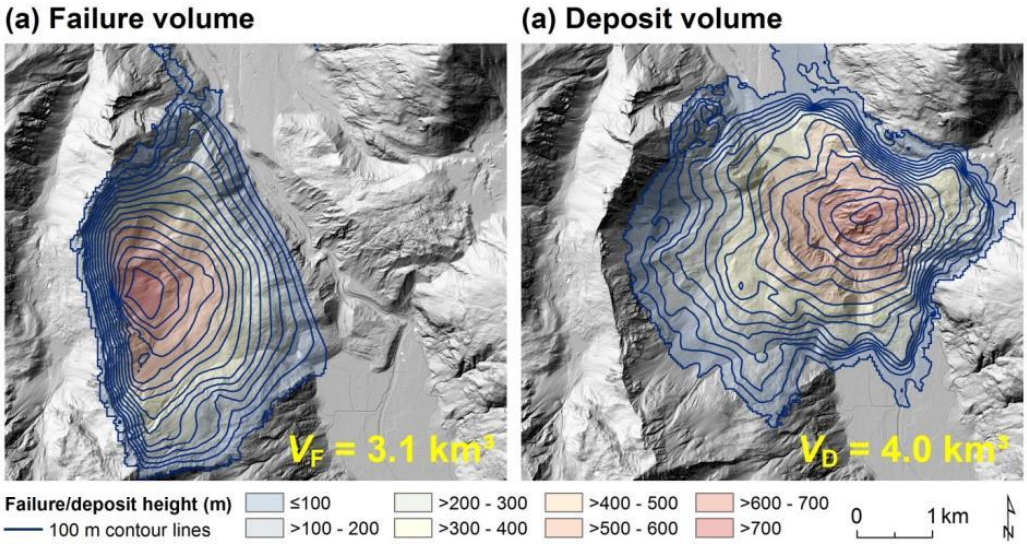

Figure 7~~8~~: (a) Failure and (b) deposition heights and volumes of the Köfels Rock Slide mass computed in ArcGIS. The contour lines indicate the height difference between the (a) pre-failure and (b) post-failure topography and the topography of the sliding surface.

955

Formatiert: Block

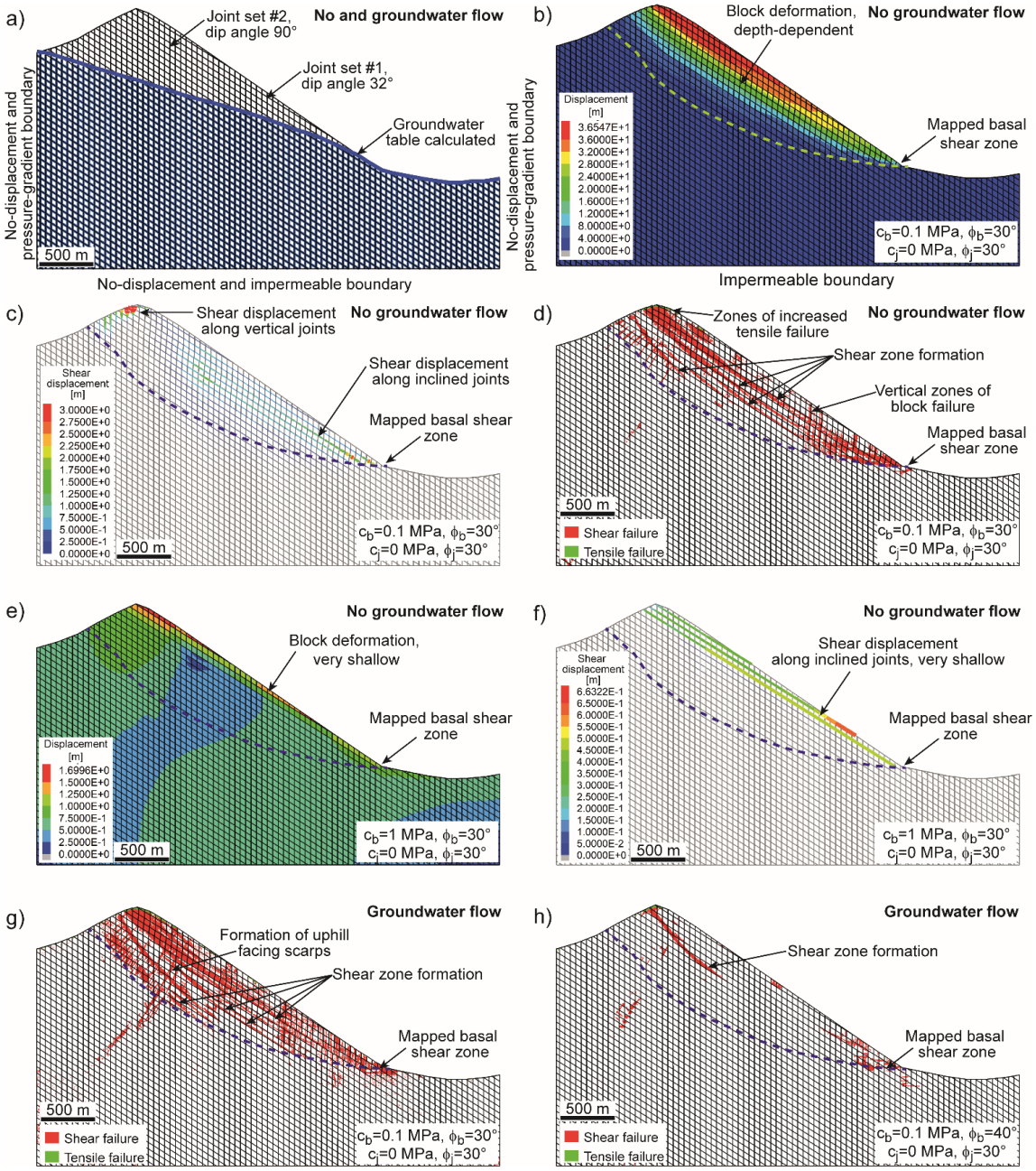
a)
No and groundwater flow
Joint set #2, dip angle 90°
Joint set #1, dip angle 32°
Groundwater table calculated
No-displacement and pressure-gradient boundary
No-displacement and pressure-gradient boundary
500 m
No-displacement and impermeable boundary
b)
No groundwater flow
Block deformation, depth-dependent
Displacement [m]
3.6547E+1
3.6000E+1
3.2000E+1
2.8000E+1
2.4000E+1
2.0000E+1
1.6000E+1
1.2000E+1
8.0000E+0
4.0000E+0
0.0000E+0
Mapped basal shear zone
cb=0.1 MPa, ϕb=30°
cj=0 MPa, ϕj=30°
Impermeable boundary
c)
No groundwater flow
Shear displacement along vertical joints
Shear displacement along inclined joints
Mapped basal shear zone
Shear displacement [m]
3.0000E+0
2.7500E+0
2.5000E+0
2.2500E+0
2.0000E+0
1.7500E+0
1.5000E+0
1.2500E+0
1.0000E+0
7.5000E-1
5.0000E-1
2.5000E-1
0.0000E+0
500 m
cb=0.1 MPa, ϕb=30°
cj=0 MPa, ϕj=30°
d)
No groundwater flow
Zones of increased tensile failure
Shear zone formation
Vertical zones of block failure
Mapped basal shear zone
500 m
Shear failure
Tensile failure
cb=0.1 MPa, ϕb=30°
cj=0 MPa, ϕj=30°
e)
No groundwater flow
Block deformation, very shallow
Mapped basal shear zone
Displacement [m]
1.6996E+0
1.5000E+0
1.2500E+0
1.0000E+0
7.5000E-1
5.0000E-1
2.5000E-1
0.0000E+0
500 m
cb=1 MPa, ϕb=30°
cj=0 MPa, ϕj=30°
f)
No groundwater flow
Shear displacement along inclined joints, very shallow
Mapped basal shear zone
Shear displacement [m]
6.6322E-1
6.5000E-1
6.0000E-1
5.5000E-1
5.0000E-1
4.5000E-1
4.0000E-1
3.5000E-1
3.0000E-1
2.5000E-1
2.0000E-1
1.5000E-1
1.0000E-1
5.0000E-2
0.0000E+0
500 m
cb=1 MPa, ϕb=30°
cj=0 MPa, ϕj=30°
g)
Groundwater flow
Formation of uphill facing scarps
Shear zone formation
Mapped basal shear zone
500 m
Shear failure
Tensile failure
cb=0.1 MPa, ϕb=30°
cj=0 MPa, ϕj=30°
h)
Groundwater flow
Shear zone formation
Mapped basal shear zone
500 m
Shear failure
Tensile failure
cb=0.1 MPa, ϕb=40°
cj=0 MPa, ϕj=30°

Figure 8: Results of modelling scenario I: a) Model set-up presenting the joint network and the calculated groundwater situation, b) depth-dependent distribution of block displacements by implementing a block cohesion of c_b=0.1 MPa, and internal friction angle of φ_b=30°, c) spatial distribution of shear displacements along joints (c_b=0.1 MPa, φ_b=30°), d) formation of multiple shear and antithetic zones due to shear failure in blocks along line-shaped zones (c_b=0.1 MPa, φ_b=30°), e) model run results when increasing the block cohesion from c_b=0.1 to c_b=1 MPa (φ_b=30°), and indicating very shallow block displacements only, f) shallow occuring shear displacements along joints for c_b=0.1 MPa and φ_b=30°, g) model run considering groundwater flow showing the formation of multiple shear and antithetic zones (i.e. uphill-facing scarps) due to shear failure in blocks (c_b=0.1 MPa, φ_b=30°), and h) model run considering groundwater flow showing the formation of a single shear initiating mainly in the summit area and at the foot of the slope, when the friction angle is increased to φ_b=40° (c_b=0.1 MPa). All model runs presented reached stabilisation.

Formatiert: Schriftart:

Formatiert: Schriftart: Kursiv, Tiefgestellt

Formatiert: Schriftart: Kursiv, Tiefgestellt

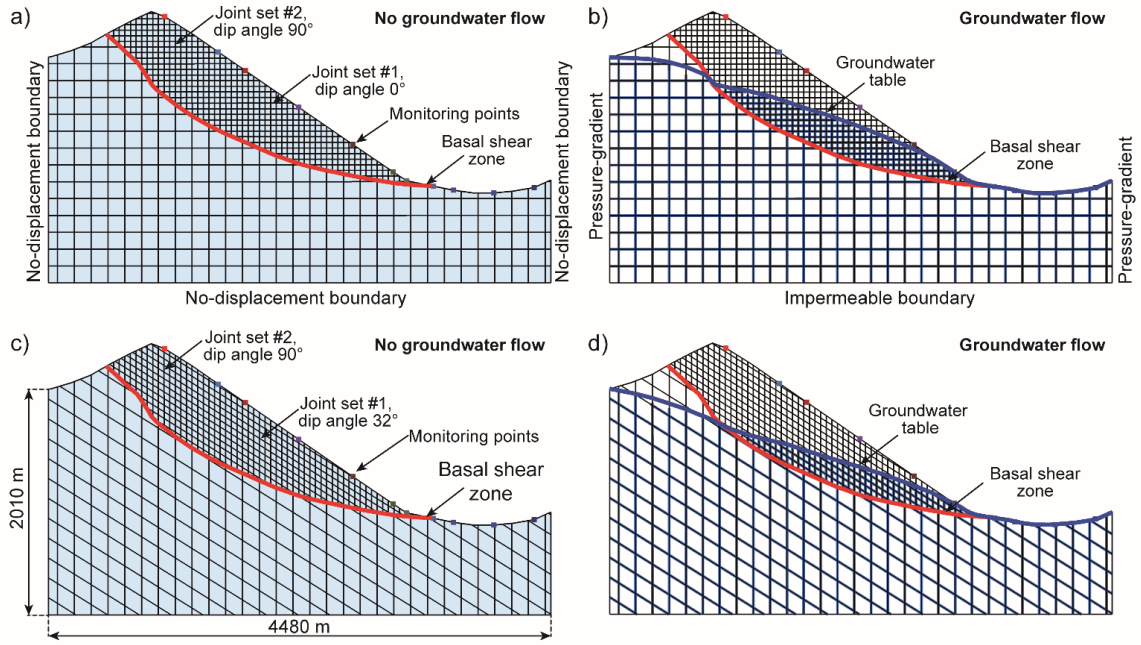

Figure 9. Model set and groundwater flow of modelling scenario II: a) model geometry characterised by a fully-persistent horizontal (dip angle 90°) and vertical joint set (dip angle 0°) and the reconstructed basal shear zone, b) same model geometry as in (a) but with considering groundater flow, c) model geometry characterised by a fully-persistent inclined (dip angle 32°) and vertical joint (dip angle 0°) set, and the

reconstruced basal shear zone, d) same model geometry as in (c) but with considering groundater flow. Monitoring points are included to prove if model runs have reached equlibrium (unbalanced forces) and stabilisation (i.e. no ongoing displacements).

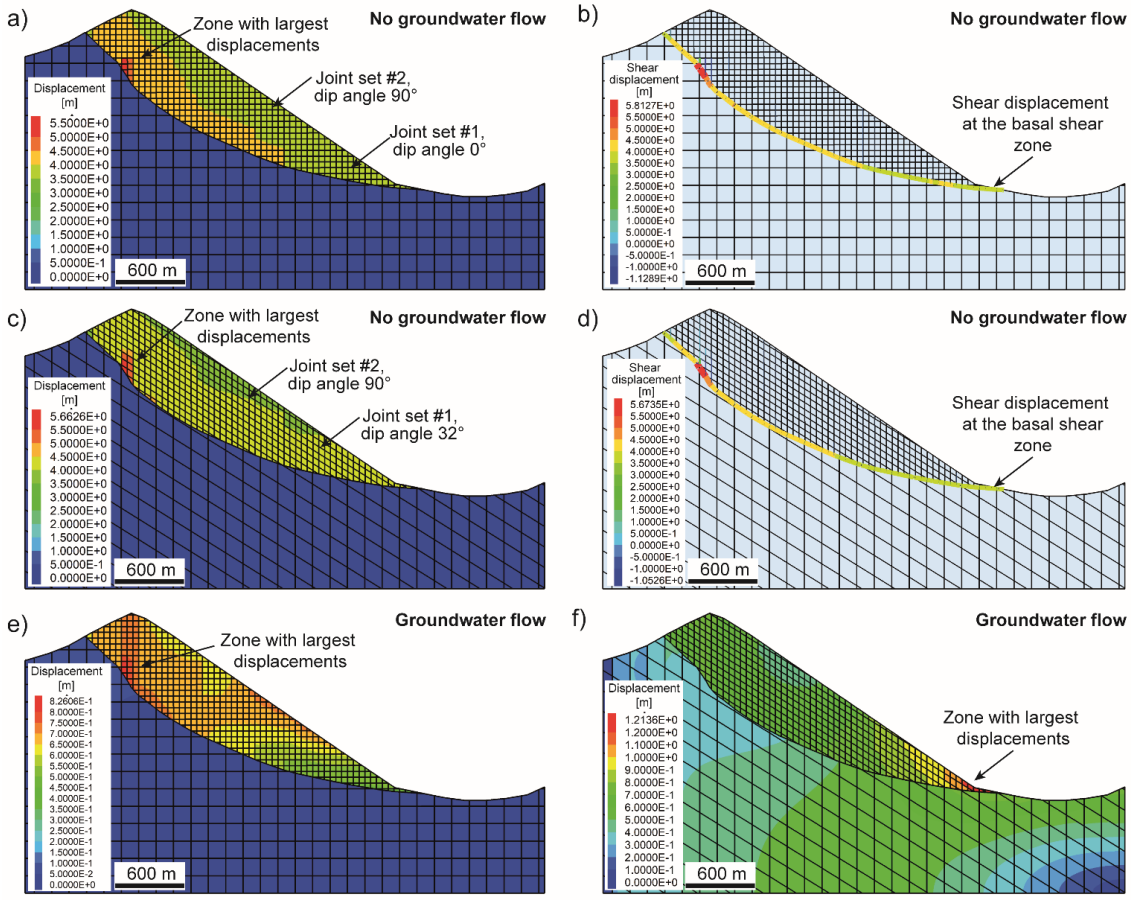

Figure 10. Results of modelling scenario II: a) internal deformation of the rock slide mass with horizontal/vertical joint sets, presented by the spatial distribution of block displacements with the maximum being around the steeply inclined section of the basal shear zone, b) spatial distribution of shear displacements along the basal shear zone for the same model type as in (a), c) internal deformation of the rock slide mass with horizontal/inclined joint sets, presented by the spatial distribution of block displacements with the maximum being around the steeply inclined section of the basal shear zone, d) spatial

distribution of shear displacements along the basal shear zone for the same model type as in (c), e) internal deformation of the rock slide mass with horizontal/vertical joint sets when groundwater flow is considered. Similar to dry conditions maximum block displacements were calaculated near the steeply inclined section of the basal shear zone, and f) internal deformation of the rock slide mass with horizontal/inclined joint sets when groundwater flow is considered. Maximum block displacements were calaculated at the foot of the slope.

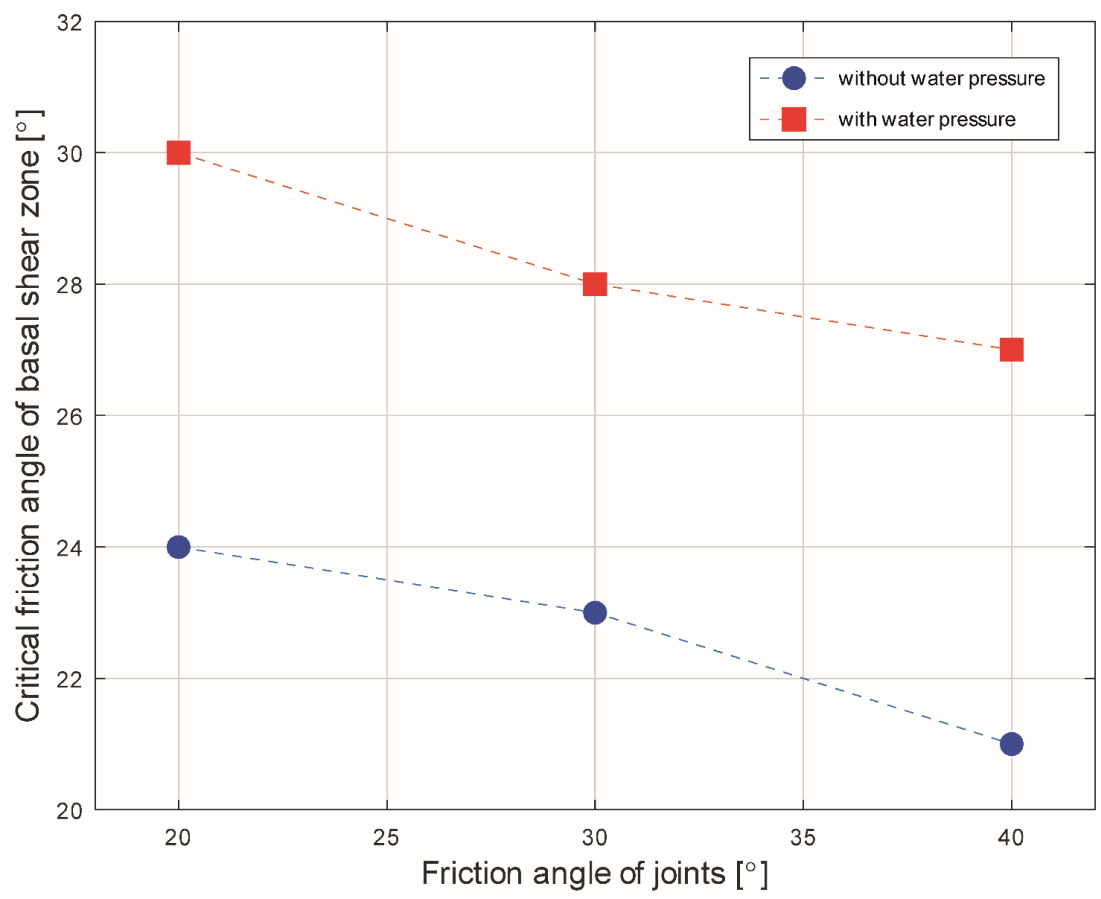

Figure 11. Relationship between the applied friction angle of the joints in the rock slide mass and the back-calculated friction angle of the basal shear zone at failure, grouped into model runs without and with groundwater flow (cohesion was set to zero for joints and the basal shear zone).

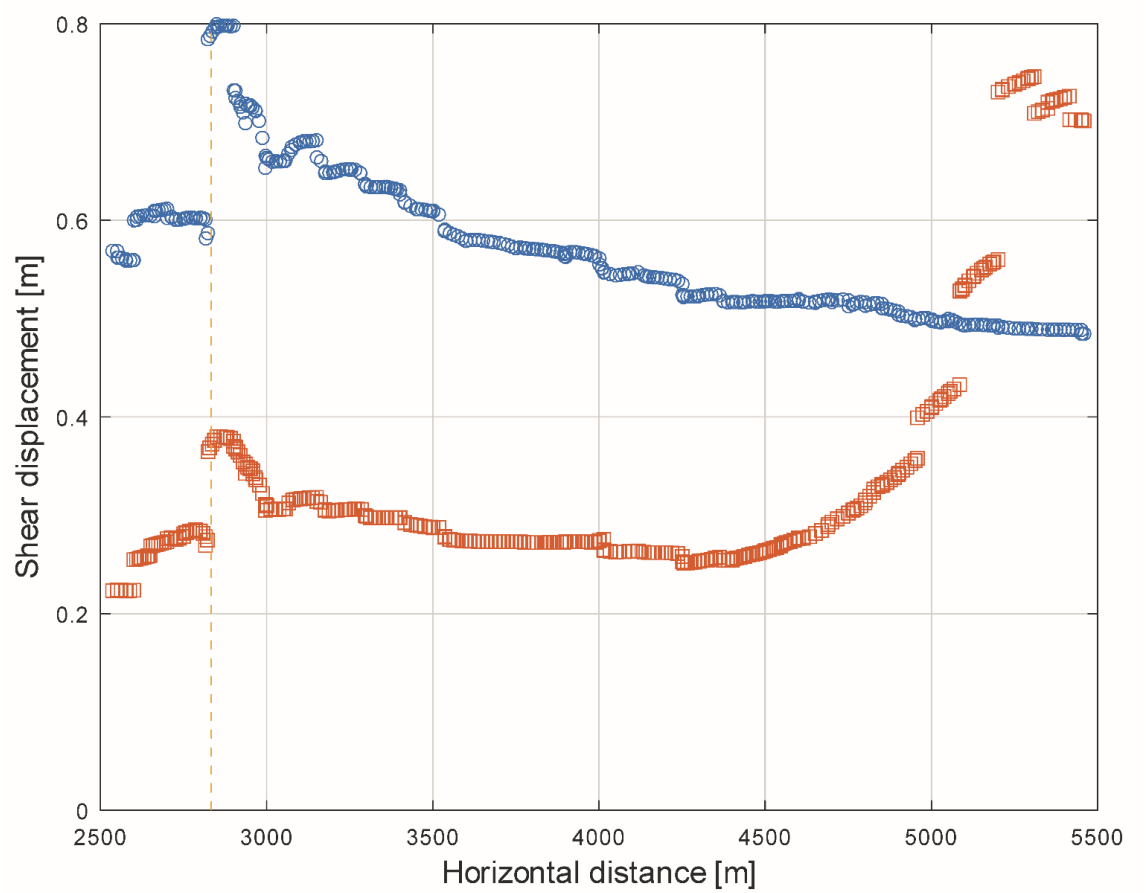

Figure 12. Different spatial distribution of shear displacement magnitues along the basal shear zone for the model types with horizontal/vertical joint sets (blue circles, see Fig. 10e) and inclined (32°)/vertical joint sets (red squares, see Fig. 10f), respectively. At model location x=2823 m, a step in shear displacement occurred due to a kink in the basal shear zone. Both model types consider groundwater flow and the joint pressure distribution can be seen in Figs. 9b, d.

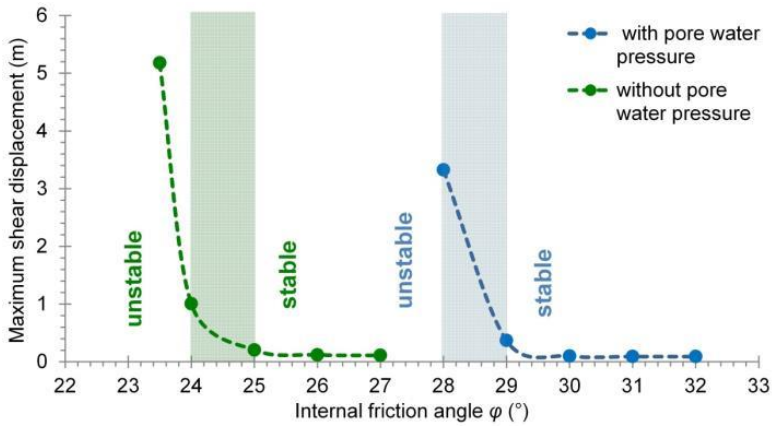

~~Figure 9: Results of the back-calculations with and without pore water pressure: the transition between failure and stable conditions without pore water pressure (scenario A) is found at φcrit = 24–25°. Applying pore water pressure to the model (scenario B) increases this transition zone to φcrit = 28–29°.~~

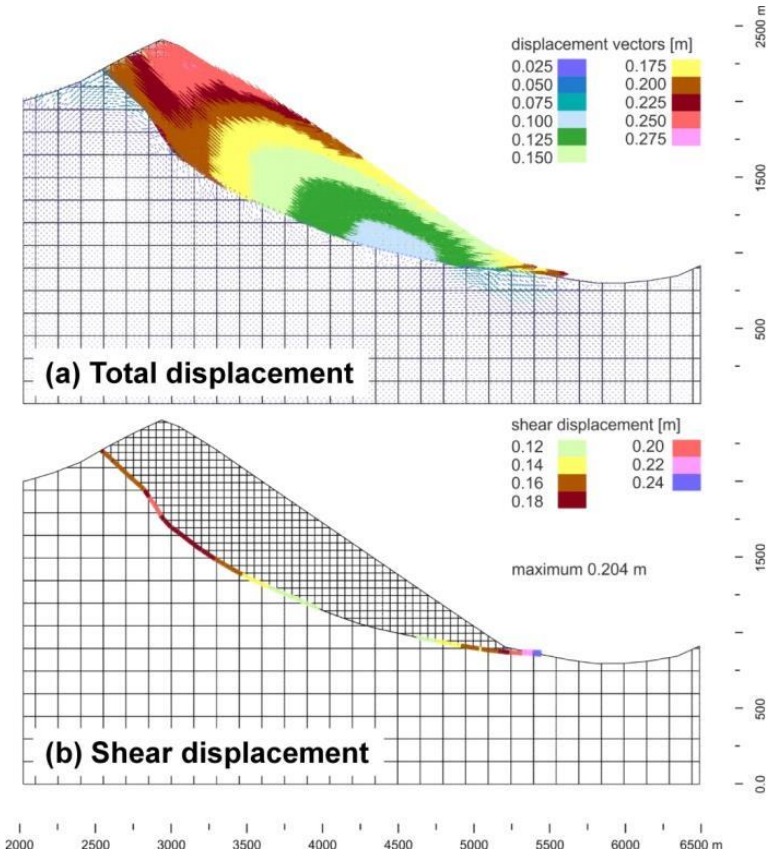

~~Figure 10: Spatial distribution of (a) total displacement and (b) shear displacement for φ = 25° for the modelling scenario (A) without pore water pressure.~~

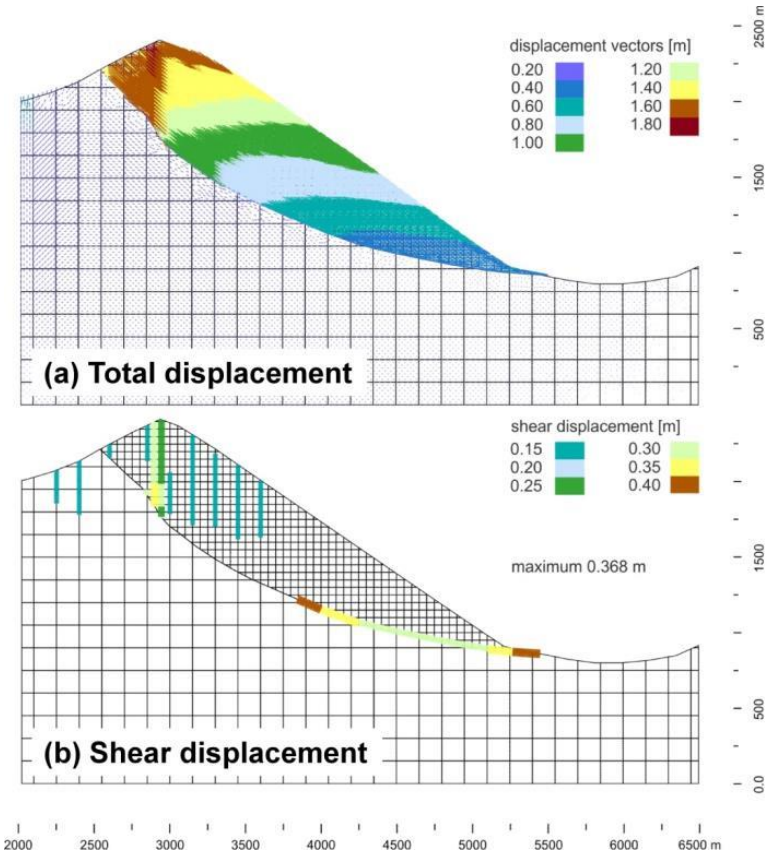

Figure 11: Spatial distribution of (a) total displacement and (b) shear displacement for $\varphi = 29°$ for the modelling scenario (B) with pore water pressure.

Tables

Table 1. Intact rock and discontinuity properties for the discontinuum distinct element analysis, categorized into rock slide mass, underlying rock mass and basal shear zone (a_{zero}, a_{res} and j_{perm} are only relevant for modelling scenario (B) considering groundwater flow, all other parameters are the same for the modelling scenarios (A) and (B)).

Material property	Rock slide mass	Underlying rock mass	Basal shear zone
Density ρ (kg/m³)	2600	2600	–
Bulk modulus K (GPa)	22	22	–
Shear modulus G (GPa)	17	17	–
Discontinuity normal stiffness j_{kn} (GPa/m)	100	100	100
Discontinuity shear stiffness j_{ks} (GPa/m)	100	100	100
Discontinuity cohesion c (Pa)	0	0	0
Discontinuity friction angle φ (°)	30	30	Varied 20–27 and 26–32
Aperture for zero normal stress a_{zero} (m)	0.00018	0.00026	0.00026
Residual aperture at shear stress a_{res} (m)	0.00018	0.00026	0.00026
Discontinuity permeability constant j_{perm} (1/Pa s)	83.3	83.3	83.3

Table 1. Rock block and discontinuity properties for the distinct element modelling study for Scenario I and II, and categorized into rock slide mass, underlying rock mass, basal shear zone, and fractured rock mass. Hydraulic parameters (a_{zero}, a_{res} and j_{perm}) are only relevant for model runs considering groundwater flow. Modelling scenario I is based solely on an elastic constitutive relationship for blocks, whereas for scenario II the blocks are simulated by applying a Mohr-Coulomb constitutive model.

Model Scenario	Scenario I	Scenario II

Material property	Fractured rock mass	Rock slide mass	Underlying rock mass	Basal shear zone
Block density, ρ [kg/m³]	2600	2600	2600	–
Block bulk modulus, K [GPa]	22	22	22	–
Block shear modulus, G [GPa]	17	17	17	–
Block cohesion, c_b [MPa]	0.1, 1	–	–	–
Block internal friction angle, ϕ_b [°]	20, 25, 30, 35, 40	–	–	–
Block tensile strength, σ_t [MPa]	0, 0.1	–	–	–
Discontinuity normal stiffness, j_{kn} [GPa/m]	100	100	100	100
Discontinuity shear stiffness, j_{ks} [GPa/m]	100	100	100	100
Discontinuity cohesion, c [MPa]	0	0	0	0
Discontinuity friction, φ_j or φ_{bs} [°]	25, 30, 35	20, 30, 40	40	20, 21, 22, 23, 24, 25, 26, 27, 28, 29, 30, 31
Hydraulic aperture for zero normal stress, a_{zero} [m]	0.00026	0.00018	0.00026	0.00026
Hydraulic residual aperture, a_{res} [m]	0.00026	0.00018	0.00026	0.00026
Discontinuity permeability constant, j_{perm} [1/Pa s]	83.3	83.3	83.3	83.3

1030